Geofluids and Mountain Building:
Integrated Isotopic Studies of Deformed, Clay-Rich Rocks

by

Erin Anne Lynch

A dissertation submitted in partial fulfillment
of the requirements for the degree of
Doctor of Philosophy
(Earth and Environmental Science)
in the University of Michigan
2018

Doctoral Committee:

Professor Ben van der Pluijm, Chair
Professor Joel Blum
Professor Aline Cotel
Professor Kyger C. Lohmann

Erin Anne Lynch

lynchea@umich.edu

ORCID iD: 0000-0002-1623-590X

Dedication

This dissertation is dedicated to my parents, Michael and Martha, who instilled in me a love of learning, and who have supported my curiosity and my adventures without hesitation. And to my sister Jamie, who has always been by my side ready to commiserate the bad times and celebrate the good.

Acknowledgements

I would like to extend my gratitude to all my colleagues, friends, and mentors who have supported me and shared experiences with me, and from whom I have learned so much during my time at the University of Michigan.

Thanks to fellow students for their support both academic and emotional: Austin Boles, Samantha Nemkin, Alyssa Abbey, Petr Yakovlev, Lydia Staisch, Mark Robbins, Sarah Walker, Joe El Adli, Tristan Childress, Xiaofei Pu, Billy Medwedeff, Chris Banner, Lindsey Abdale, Sam Haugland, Ross Maguire, Kate Volk, Brian Konecke, Anna Woodson, Alex Rand, Walt Afonso Andrew Gerlach, Kyle Meyer, Neal Hughes, Aaron Kurz, Katy Rico.

Thanks also to collaborators, colleagues, and faculty to whom I attribute much of my intellectual growth: Sam Haines, Andreas Mulch, Torsten Vennemann, Adolph Yonkee, Benita Putlitz, Chris Hall, Marcus Johnson, Jerry Zhongrui Li, Anja Schleicher, Brice Lacroix, Nathan Neimi, John Geissman, Adam Simon, Rob Van der Voo, Dinu Pana, Udo Becker, Nathan Sheldon, Eric Hetland, with extra thanks to my committee members Joel Blum, Aline Cotel, and Kyger Lohmann for their feedback and for keeping me on track.

And of course, I thank my advisor, Ben van der Pluijm, for his persistence and patience getting through to the end of each project we tackled, and for his sense of humor and general life encouragement that complemented that academic guidance.

I am grateful for the funding that has supported my research, which included many Scott Turner Research Grants and the Susan M. Kruger fellowship from the Earth and Environmental Sciences department and a Predoctoral Fellowship from the Horace H. Rackham School of Graduate Studies. I am thankful for additional funding that was provided through research and travel grants from the Rackham Graduate School, the Geological Society of America, the Clay Minerals Society, the Society of Economic Geologists, and the National Association of Geoscience Teachers.

Lastly to my family, for their unwavering support, encouragement, and love, thank you.

Table of Contents

List of Figures

phase. Patterns are collected from oriented ethelyne glycol air-saturated samples to swell smectite interlayers. Characteristic (hkl) peaks of smectite are shown at top. K = kaolinite, present at near detection limits in WH68-3 (MF). C) Gouges where chlorite is the dominant clay mineral in the gouge. The chlorite is fragmental, derived from chlorite-epidote microbreccia footwall lithologies, and is not neoformed in the gouge. Patterns are collected from random-mounted patterns to highlight higher-order (hkl) reflections and polytype-specific peaks. Characteristic (hkl) peaks for chlorite are shown at top. I = 10 Å mica (illite, muscovite, or biotite) present in near-detection limit quantities in samples A-BOMB 3 (M) and MOR-3 (M). C = calcite, present in near-detection limit amounts in sample MOR-3 (M). Note that for all samples, (F) in sample name indicates size fraction <0.05 μm (Stokes equivalent). (M) = 0.2 – 0.05 μm size fraction. (MF) = <0.2 μm size fraction. Note that by contrast, (G) in a sample name refers to the green color from chlorite and does not connote a size fraction. BAD-1 (G) is a <0.2 μm size fraction. **160**

Figure A.5: $\delta^{18}O$ and $\delta^{2}H$ values of neoformed low-angle normal fault (LANF) gouge illite, smectite, and chlorite, together with calculated fluid compositions exchanging with each phase. (A) Fault-gouge illite isotopic values plotted together with isotopic data from illites from other geological environments for reference. Illite geological environment data are compiled from references in Data Repository Files DR5 and DR6. Uncertainties for all $\delta^{18}O$ and $\delta^{2}H$ measurements are within sample marker point size. Fault-gouge illite results: *S*—Savcili fault, Turkey (Isik et al., 2014); *NA*—North Anatolian fault zone, Turkey (Tonguç Uysal et al., 2006); *M*—Moab fault, Utah, USA (Solum, 2005). (B) Range of calculated fluid compositions of exchanging fluid for illites. Fluid compositions are calculated using fractionation equations of Sheppard and Gilg (1996) and Capuano (1992).Temperatures are bounded on the lower limit by 50 °C or the meteoric water line and on the upper end at 120 °C by the observed upper temperature limit for illite-rich illite-smectite in sedimentary basins. (C) Fault-gouge smectite isotopic values plotted together with isotopic data from smectites from other geological environments. Smectite geological environment data are compiled from references in Data Repository Files DR5 and DR6. (MF) indicates <0.2 mm size fraction. (D) Calculated fluid compositions of exchanging fluid for smectites. Fluid compositions are calculated using fractionation equations of Sheppard and Gilg (1996) and Capuano (1992).Temperatures are bounded on the lower limit by 50 °C or the meteoric water line and on the upper end at 120 °C. (E) Fault- gouge chlorite isotopic values plotted together with isotopic data from other geological environments for reference. Chlorite geological environment data are compiled from references in Data Repository Files DR5 and DR6. Fault or shear zone chlorite results: WO—Walter-Outalpa shear zone, Australia, Alice Springs orogen, Australia, and Argentera massif, France (Clark et al., 2006; Raimondo et al., 2011; Leclere et al., 2014); *A*—Alpine fault (Menzies et al., 2014); *P*—Picacho metamorphic core complex (Kerrich and Rehrig, 1987); *MP*—Monte Perdido thrust, Spain (Lacroix et al., 2012). (F) Calculated fluid compositions of exchanging fluid for chlorites. Fluid compositions are calculated using fractionation equations of Cole and Ripley (1998) and Graham et al. (1987). Because significant uncertainties exist for the magnitude of chlorite-

List of Tables

List of Appendices

Abstract

Hypotheses on the origins and pathways of geofluids in Earth's crust are numerous and conflicting, ranging from the release of volatiles from magmatic and metamorphic bodies to km-scale infiltration of surface waters. In contractional orogens, the release of metamorphic fluid from the orogenic core would be expected to cause fluids to travel towards the low-temperature and low-pressure foreland region. Alternatively, the high elevation of the orogenic core could allow surface-sourced meteoric fluids to infiltrate the crust and gravitationally travel toward the foreland. These two primary fluid sources have unique stable isotopic signatures, which they impart to minerals that precipitate as a result of their passing. By investigating the isotopic signatures preserved in secondary clay minerals, this dissertation examines the origin of ancient fluids in four fold-and-thrust belts. Both hydrogen and oxygen isotopes are used to examine the provenance of deformational fluids, while $^{40}Ar/^{39}Ar$ dating is used to constrain the timing of fluid passage and mineralization. These integrated stable and radiogenic isotopic techniques explore the characteristics of several mountain chains from different locations in North and South American and different periods of geologic time from the Paleozoic to the Cenozoic. Stable hydrogen isotopes in fault gouge of the Argentine Precordillera show that fault rock fluids preserve signals of the aridifying Miocene climate in Central South America. Comparing the hydrogen isotopic signature in deformational clays in the Sevier fold-thrust belt of the North American Cordillera to the isotopic proxies of ancient surface fluids shows that clays track the isotopic

composition of low-elevation surface fluids in the late Mesozoic. Combining oxygen and hydrogen isotope analyses in the Canadian Cordillera of Alberta on previously dated clay gouge shows variable mixing of metamorphic fluids and high-latitude meteoric fluids. Lastly, paired stable and radiogenic isotope studies and dating of clays from the Late Paleozoic Central Appalachian orogen reveal similar mixing of metamorphic and isotopically buffered meteoric fluids.

Appendix A represents the early development and application of paired H-isotopic analysis and Ar-dating, showing that ancient meteoric fluids dominate Basin and Range crust during relatively young tectonic extension. Appendix B describes the Ar-dating correction procedure that corrects a subset of erroneous sample size fractions in Chapters III and V. Appendix C describes a preliminary comparison with Southern Appalachian fault gouge clay isotopic composition, revealing both the dominance of metamorphic fluid signatures in some areas and the mixing of meteoric and metamorphic fluids in others. Lastly, Appendix D explores a novel application of mercury isotopes to deformation fluid studies in samples San Andreas Fault cores, indicating that mercury isotopes are not a unique tracer of fluid sources in these samples, but they may be used to constrain the fluid sources and fractionation processes that occur in crustal rock reservoirs.

This set of studies shows that ancient, meteoric fluids play an important role in upper crustal deformation. The mixing of metamorphic and meteoric fluids implies an open fluid system and a balancing of driving forces, gravitational and buoyancy forces, which together promote foreland-directed fluid flow in compressional tectonic belts.

Chapter I. Introduction

The tectonic evolution of our planet is dynamic. Though tectonic plates are often thought of as rigid blocks of rock jostling and bumping each other along narrow boundaries, causing earthquakes and creating volcanoes, crustal deformation is a complex system involving several components. Of course, lithology is a major element in these systems, but rock properties change with depth at increasing pressures and temperatures, such that rock deformation at the surface is quite different than deformation at depth. Another major component of crustal systems is the involvement of geologic fluids. The presence of fluids, particularly in the upper crust, facilitates rock deformation by decreasing the effective magnitude of crustal stresses and reducing frictional resistance to sliding along fault planes and bedding planes. Additionally, fluids mediate the transfer of dissolved chemical species and heat through migration and convection.

The evidence for fluid passage in rocks is abundant, including the concentration and deposition of secondary minerals, the chemical and physical alteration of host rocks, and changing crustal stress state as observed with the increasing prevalence of injection-induced earthquakes. Fault zones act as conduits for fluid flow in the crust (Moore and Vrolijk, 1992; Muir-Wood and King, 1993; Caine et al., 1996; Faulkner et al., 2010). Deformation zones around faults often show signs of alteration of the host rock and an abundance of fluid-grown mineral populations in the form of veins and clay minerals (Taylor, 1974; Kerrich, 1986; Rye and Bradbury, 1988; De Caritat et al., 1993; Vrolijk and van der Pluijm, 1999; Zwingmann et al., 1999; Swanson et al., 2012). These veins

can host deposits of economically valuable mineral ores (Craw et al., 2002; Micklethwaite and Cox, 2004). Not all mineral ores are confined to fault zones, however, fluid flow also occurs in porous sedimentary units, such as sandstones, which act as reservoirs for hydrocarbons and hydrous fluids alike. Despite their low porosity, evidence also exists for fluid flow within clay-rich sedimentary units, such as shales (Glasmann et al., 1989; Monteiro et al., 2012; Fitz-Diaz et al., 2014). Wholesale passage of fluids through sedimentary units, notably carbonates, has been hypothesized as a driver for late-stage rock remagnetization (Van der Voo, 1979; Miller and Kent, 1988; Lu et al., 1990; Stamatakos et al, 1996; Cederquist et al., 2006).

Much of our current understanding of geofluids and the conditions of migration and trapping come from the study of near-surface hydrology, oil-gas exploration, and economic geology. It is understood that faults can act as anisotropic flow controllers, providing both conduits for along-fault flow and creating barriers for across-fault flow (Moore and Vrolijk, 1992; Caine et al., 1996; Moretti et al., 2002). The directionality of fluid flow, however it may be mediated by fault orientation, is driven by other processes. Gradients in temperature and/or pressure conditions can drive fluid from regions of higher temperature/pressure towards regions of lower temperature/pressure (Oliver, 1986; Fyfe and Kerrich, 1985; Koons and Craw, 1991; Ferry, 1994; Sibson, 1994; Lyubetskaya and Ague, 2009). Gravitational forces also drive fluids from regions of high elevation towards regions of lower elevation (Garven, 1985; Deming, 1994; Garven, 1995). Lastly, the source of fluids remains a topic of spirited debate, involving deep sources, syn-depositional fluids and surface fluids. Fold-thrust belts represent a key area of study to test these hypotheses, which is the focus of this dissertation.

Fold-Thrust Belts

Fold-thrust belts are a ubiquitous feature of contractional mountain belts around the world. Typically they are found on the foreland side of orogens, and comprise a relatively thin package of pre- and syn-sedimentary units that are deformed (generally below greenschist facies metamorphic conditions) (Boyer and Elliot, 1982; Marshak and Wilkerson, 2004). In an orogenic system, fold-thrust belts are bordered on one side by the high-temperature/pressure metamorphic core of the mountain belt, and on the other side by relatively undeformed foreland basins (Figure I.1). Fold-thrust belts are bounded at their base by a shallowly dipping (<10°) décollement, or floor thrust, on top of which the sedimentary units displace and deform in a series of faults and folds. In cross-section, fold-thrust belts are generally wedge-shaped, thinning toward the foreland (Davis et al., 1983; Dahlen et al., 1984).

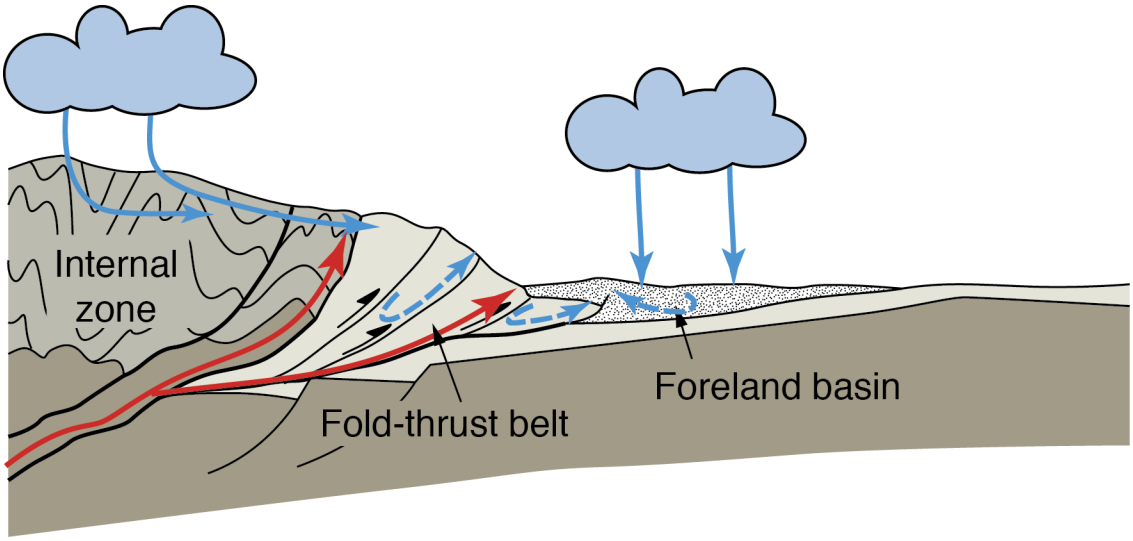

Figure I.1 Schematic diagram of a fold-thrust belt bounded by a high-P/T internal orogenic zone on the left and a foreland sedimentary basin on the right (modified from Marshak and Wilkerson, 2004). The red arrows show the proposed source (deep within the orogenic core) and pathways of upward and foreland-ward migrating of metamorphic geofluids. The solid blue arrows show the input of meteoric fluids from both high- and low-elevation sources. The dashed blue arrows show the local source of formational fluids, which may be derived from seawater or meteoric fluids.

The formation of fold-thrust belts has proven difficult to reconcile with rock mechanics and the conditions of fracturing and faulting of the thrust wedge. In a seminal paper, Hubbert and Rubey (1959) proposed a mechanism to explain how large packages of rock can be transported long distances over shallowly-dipping décollement faults. The authors called upon an increase in fluid pressure within the décollement to reduce the effective normal stress on the fault plane, allowing the fault to slip at low angles. This hypothesis, though elegant in its simplicity, necessitates that high fluid pressures be produced and maintained at depth within an evolving fold-thrust belt, and evidence for such high fluid pressures has been difficult to find. The source of these proposed fluids has also been elusive, with both metamorphic and meteoric fluids suggested as the primary fluid present at mid to shallow crustal depths (Figure I.1). Another major hypothesis is that fluid-mediated formation of low-friction minerals, such as clays, promote low-friction slip on thrust faults (e.g. Vrolijk and van der Pluijm, 1999; Vannucchi et al., 2003; Schleicher et al., 2010; Warr et al., 2014). The structural and stratigraphic heterogeneity of fold-thrust belts make simple conclusions about bulk regional hydraulic properties difficult, but understanding the fluid *identities* in fold-thrust belts can give insight into the hydraulic regime at depth and across broad regions of crust.

The Metamorphic Fluid Hypothesis

The release of deeply-sourced metamorphic fluids (and deep basinal fluids equilibrated at metamorphic temperatures) has been proposed as a source of high-pressure geofluids in crustal rocks and fault zones (Etheridge et al., 1984; Fyfe and Kerrich, 1985; Craw, 1988; Koons and Craw, 1991; Hüpers et al., 2017). Starting in greenschist facies (~300°C), prograde metamorphic reactions liberate volatile species

from crystal structures in the form of H_2O, CO_2 and other volatiles. The volume of fluid released increases with increasing pressure and temperature. Volatile production in fine-grained pelitic, or clay-rich, rocks is calculated to be ~18mL per kg of rock material that passes through the 600°C isotherm (Walther and Wood, 1984), or roughly equivalent to 3-6 weight % fluid (Peacock, 1989; Connolly, 2010). The fluid released at these depths may mix with trapped high-temperature formation fluids and is thought to travel along grain boundaries for short distances until reaching a through-going crustal structure, such as a fracture or fault, along which it can channelize and migrate quickly down-temperature/pressure to the surface (Walther and Orville, 1982; Etheridge et al., 1983; Craw, 1988; Rice, 1992; Byerlee, 1993; Connolly, 1997). Shallow décollements and deformation systems within fold-thrust belts may be one of the primary pathways for metamorphic fluids to escape to the surface.

Metamorphic fluids are inherently high-pressure fluids, and it has been theorized that metamorphic fluid release may provide the fluid pressure needed to reduce the normal stresses on fault planes, allowing them to slip at lower critical stresses (Etheridge et al., 1983; Craw, 1988). Evidence for transient high pressure in fault zones has been shown in fault zones (Rice, 1992; Sleep and Blanpied, 1992; Sibson, 1992; 1994). Blanpied et al. (1992) suggested that mineralization during the seismic cycle causes the self-sealing of faults, which allows episodic increases in fluids pressure along fault zones. Because fault zones are heterogeneous and this process is discontinuous, fluids can move longitudinally from compartments of high- to low-pressure during faulting resulting in a significant lateral component to metamorphic fluid flow (Bailey, 1990; Byerlee, 1993; Ferry and Gerdes, 1998). Additionally, because these fluids originate from depth, their

thermal qualities allow for the efficient transport of dissolved metals and economic ores. The metamorphic hypothesis implies that high-pressure (lithostatic) fluid is produced at depth in the Earth's crust, facilitating deformation and providing necessary conditions for mineralization.

The Meteoric Fluid Hypothesis

The meteoric fluid hypothesis requires that fluids at surface conditions penetrate downward into deforming crust. The infiltration of surface-sourced fluids is driven primarily by gravitational flow, with fluids penetrating the crust through fractures and faults (Garven, 1985; Deming, 1994; Garven, 1995; Ge and Garven, 1994). Zoback and Townend (2001) suggested that fractures in the brittle upper crust (perhaps up to 12km depth) allow the upper crustal hydraulic regime to be completely dominated by fluids at hydrostatic pressure. The presence of meteoric or surface-sourced fluids is known in extensional systems (Muir-Wood and King, 1993; Sibson, 1994; Mulch et al., 2004; Person et al., 2007; Campani et al., 2012; Gébelin et al., 2013; Appendix A); however, their role in compressional systems is heavily debated.

Studies of multiple generations of veins in compressional belts indicate that fluid sources may change throughout an orogenic cycle (Moore and Vrolijk, 1992; McCaig et al., 1995; Travé et al., 2007; Sample, 2010; Evans et al., 2012; Lacroix et al., 2014). Locally-sourced fluids dominate early stages of orogenic evolution, with input from externally-sourced fluids coming later in the cycle during increased deformation and fluid mobility (e.g. Travé et al., 2007). Some evidence suggests that meteoric fluids can be the dominant fluid source in the late stages of the orogenic cycle; however, understanding how and when they infiltrate the crust remains uncertain (Burtner and Nigrini, 1994;

Bebout et al., 2001; Wiltschko et al., 2009; Chapter 2). It is hypothesized that increased elevation of evolving mountain belts can drive meteoric fluids from the high-elevation orogenic core towards the lower elevation foreland (Burtner and Nigrini, 1994; Craw et al., 2002; Person et al., 2007; Wiltschko el al., 2009). A meteoric fluid source, in summary, requires that sub-lithostatic pressures can drive fluid into a deforming upper crust, perhaps all the way down to the brittle-plastic transition, and that sufficient permeability exists in compressional systems. The infiltration and migration of meteoric fluid also requires open-system behavior, which would be contrary to the hypothesis that volumes of trapped, high-pressure fluids at depth are needed to explain fold-thrust belt propagation.

Objective of the Dissertation

The objective of this dissertation is to determine the identity and source(s) of mineralizing fluids, thus providing evidence in support of one or both of the two hypotheses described above. Such evidence for fluid involvement and pathways in fold-thrust belt settings is key to our understanding of both fold-thrust belt dynamics and resource distribution.

Approach of the Dissertation

Isotopic studies of neomineralized (secondary) clay minerals are used to determine the identity(ies) of mineralizing fluid(s) in fold-thrust belts. Clay minerals are low-temperature hydrous phyllosilicates that form in a variety of geologic environments, starting at sub-metamorphic grades (e.g. de Segonzac, 1970; Hunziker, 1986; Vrolijk and van der Pluijm, 1999; Pevear, 1999). Studies have shown that clay minerals grow during deformation, both along faults and within folded, clay-rich sedimentary units (Vrolijk and

van der Pluijm, 1999; Haines and van der Pluijm, 2012; Fitz-Diaz and van der Pluijm, 2013). Unlike the majority of rock-forming minerals, clay minerals contain structurally bound hydroxyl groups, making them suitable for isotopic studies of both oxygen and hydrogen (Figure I.2); the latter will be key to our interpretations. Whereas water in the clay interlayers easily exchanges with the ambient fluids or atmospheric vapor, structurally bound OH- groups within the mineral lattice do not. Instead they are robust recorders of the isotopic composition of their formation and the originating fluid(s). Additionally, illitic clay minerals contain radioactive potassium, which allows the timing of their formation to be determined using modern $^{40}Ar/^{39}Ar$-dating on very small samples sizes.

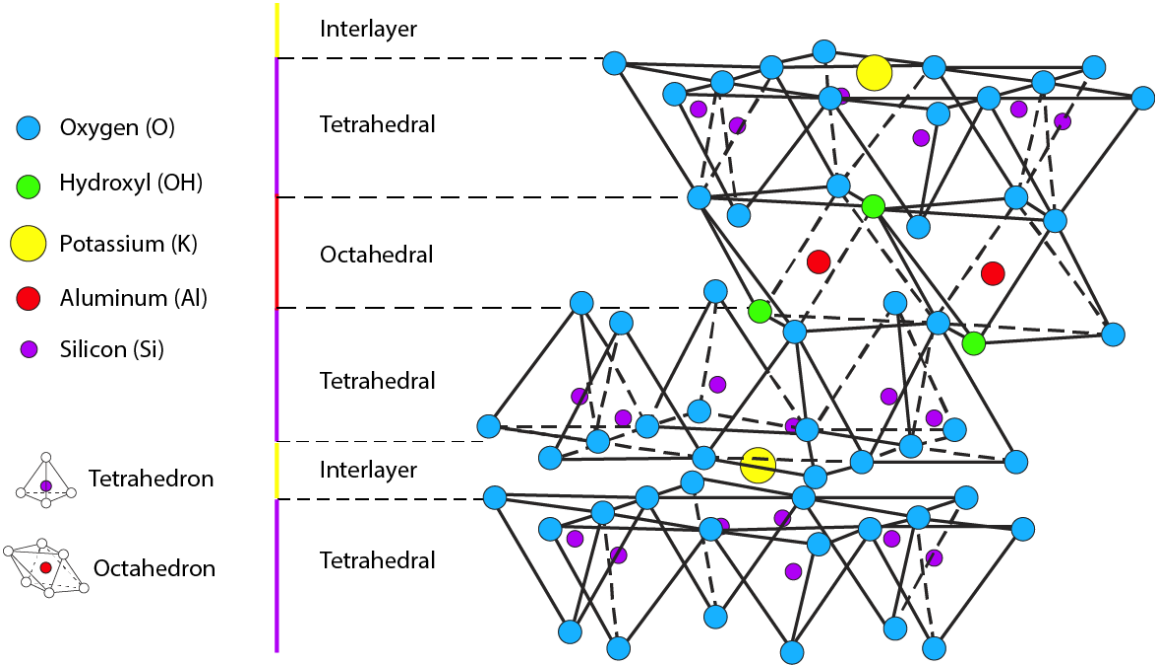

Figure I.2: The structure of the clay mineral illite consists of a series of stacked sheets. Each sheet has an octahedrally coordinated layer sandwiched between two tetrahedrally coordinated layers with Aluminum and Silicon as the major cations. OH- groups (green) are contained inside the crystal structure, within the octahedral layer. K^+ ions balance the negative charge in the sheets by occupying the interlayer spaces between them (yellow). (Modified after Grim, 1962)

Stable Isotopic Analysis

The distribution of stable isotopes in crustal reservoirs is used to understand processes and environments (e.g. Taylor, 1974; Sheppard, 1986). For instance, stable isotopic studies of secondary minerals in soils/paleosols and in fossils have led to understanding of past climate and elevation regimes (e.g. Lawrence and Taylor, 1971; Dettman and Lohmann, 1993; Koch et al., 1995; Poage and Chamberlain, 2002; Mulch et al., 2010; Chamberlain et al., 2012; Peters et al., 2013; and many others). In fold-thrust belts, stable isotopic studies of silicate and carbonate veins and fluid inclusions have produced abundant evidence for fluid involvement in deformational processes (e.g. Rye and Bradbury, 1988; Evans and Battles, 1999; Bebout et al., 2001; Kirshner and Kennedy, 2001; Fitz-Diaz et al., 2011; Evans et al., 2012). Most of these stable isotopic studies, however, rely on the oxygen isotopic signatures of various proxies, due to the abundance of oxygen in the geologic materials. Studies exploring hydrogen isotopes in the geologic record have been restricted primarily to the analyses of fluid inclusions and much less, as in this dissertation, to hydrous minerals.

Clay minerals provide the opportunity to explore the identity and role of geofluids through the lens of *both* hydrogen and oxygen isotopic signatures in upper crustal environments. Because geofluids have unique oxygen and hydrogen isotopic signatures (denoted as $\delta^{18}O$ and δD, respectively; Figure I.3), the stable isotopic signatures preserved in the rock record can be used to identify the relative contribution of different fluid sources. Metamorphic fluids have high $\delta^{18}O$ and δD values, whereas meteoric fluids have low $\delta^{18}O$ and δD values; seawater has low $\delta^{18}O$ and high δD (Taylor, 1974; Sheppard, 1986). Using geologic temperature constraints and well-established clay-water

fractionation behavior, calculations of the mineralizing fluid composition can be made, allowing conclusions regarding the identity and history of those fluid sources.

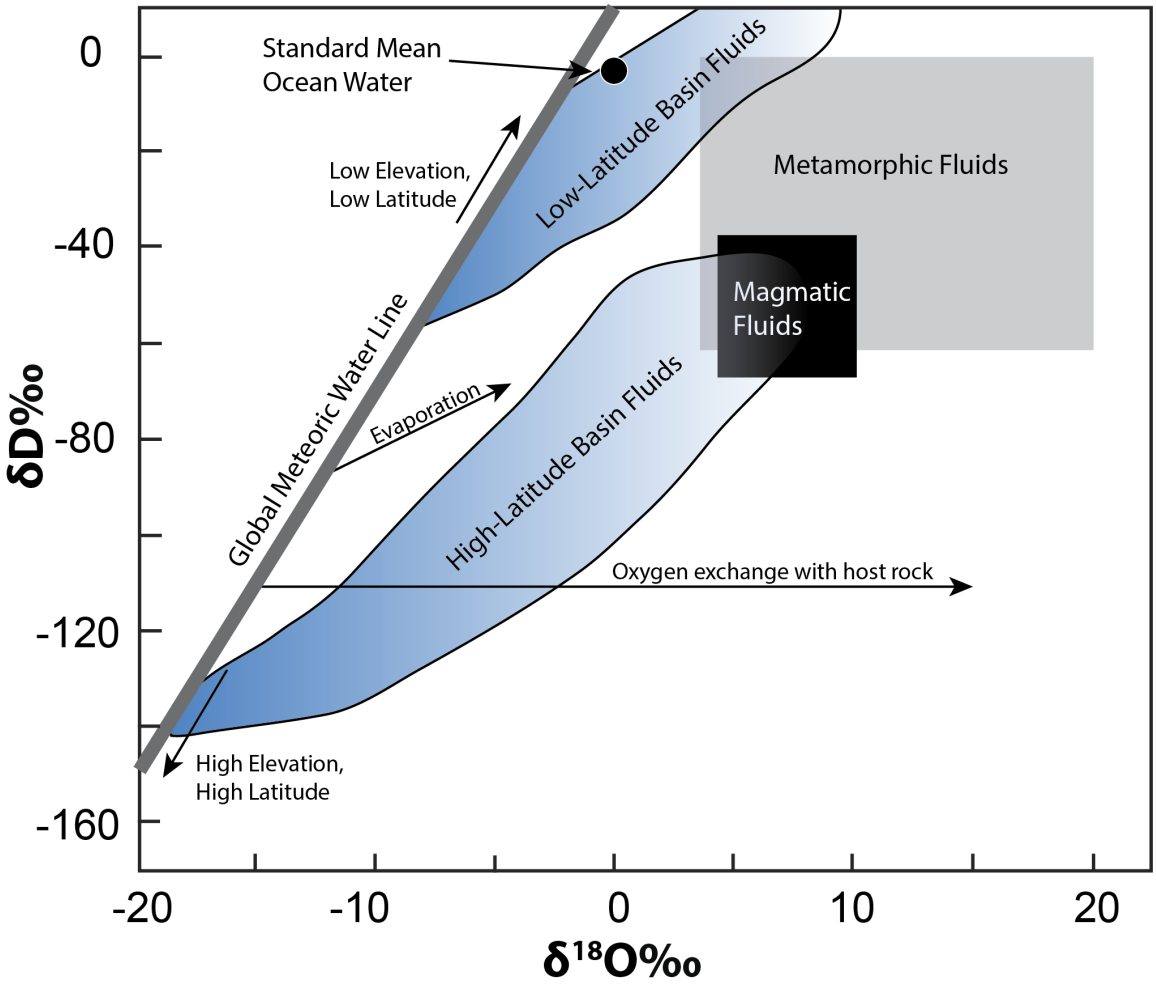

Figure I.3: Stable isotopic composition of major crustal fluids (modified after Sheppard, 1986). The grey box shows the average composition of metamorphic fluids; the black box shows magmatic fluid composition. The dark grey line, the global meteoric water line, shows the range of composition of meteoric fluids, with high elevation, high latitude fluids towards the negative end of the line, and low elevation, low latitude meteoric fluids towards the less negative end of the line. Standard mean ocean water (SMOW) is shown as a large black dot at the origin, and represents the standard isotopic composition to which all fluids are compared. Blue shaded fields represent basin waters from different sedimentary basins around the world. These waters often originate as meteoric or ocean water and are modified in their isotopic composition by their interaction with the host rock and through evaporative enrichment (both processes are indicated with black arrows).

Radiogenic Isotopic Analysis

The potassium-rich clay mineral illite is highly suitable for $^{40}Ar/^{39}Ar$-dating of low-temperature processes, including folding and faulting in the upper crust (e.g. Dong et al., 1997; Pevear, 1999; van der Pluijm et al., 2001; Rahl et al., 2011; Clauer et al., 2012; Fitz-Diaz and van der Pluijm, 2013). Particularly, radiometric dating of neoformed illite, paired with stable isotopic analysis, allows both for the identification of fluids involved in deformation and mineralization and the timing of fluid activity.

Outline of the Dissertation

This dissertation consists of multiple studies of fold-thrust belts in North and South America, ranging in age from the Paleozoic (Appalachians) to the Neogene (Andes). Three studies from the American Cordillera (Andes, Sevier, Canadian Cordillera) and two from the Appalachian Mountains (Central and Southern) allow for the comparison of ancient geofluid input at different latitudes and different ages along the orogenic systems.

Chapter II, published in *Lithosphere* by Lynch and van der Pluijm (2016), explores the hydrogen isotopic composition of fault gouge from Central Andes in Argentina. Results indicate that the isotopic signatures recorded in the fault gouge parallel the isotopic record elsewhere in the Central Andes region, tracking the aridification associated with the warming Miocene climate. Chapter II concludes that surface-sourced fluids, rather than metamorphic fluids, mediated Miocene faulting. Furthermore, Chapter II suggests that studies of fold-thrust belt fault fluids can be used as paleoclimate proxies.

Chapter III, submitted to *Earth and Planetary Science Letters* by Lynch et al., (*in review*), combines hydrogen isotopic studies with clay dating methods in the Sevier fold-thrust belt of Idaho and Wyoming. As in Chapter II, hydrogen isotopic signatures in clay minerals complement existing oxygen isotopic proxies for paleoclimate/paleoprecipitation in the Cretaceous/Paleogene of western North America. This observed fluid signature contrasts markedly with the isotopic composition of present day precipitation. $^{40}Ar/^{39}Ar$-dating of fine-grained authigenic clay minerals constrains the growth of the clays as Mezosoic, and, therefore, characterizes the Mesozoic identity of mineralizing fluids.

Chapter IV combines stable isotopic studies of previously dated clay minerals including oxygen along with hydrogen in the Canadian Rockies. The hydrogen isotopic composition of clay minerals shows a spread, suggesting the mixing of fluid sources. Using a combination of two isotopic systems allows us to calculate the relative volume of each fluid source involved in thrusting. Combining oxygen and hydrogen, we determine that the average fault fluid typically has a 50%/50% mix of metamorphic and surface-sourced fluid, with some fluids containing as much as 75% metamorphic or 75% surface-sourced fluids. In contrast to the results in chapters II and III, this indicates that metamorphic fluids can make up a significant portion of the geofluid budget of fold-thrust belts.

Chapter V applies the isotopic approaches of the previous chapters to the Appalachian orogen: stable isotopic studies of oxygen and hydrogen, and $^{40}Ar/^{39}Ar$ clay dating. As in the Canadian Cordillera (Chapter IV) we find that both metamorphic and surface-sourced fluids are involved in fold-thrust belt deformation. Insight from oxygen

isotopic composition of the clay mineralizing fluids suggests that oxygen isotopic buffering with host rock units was a contributing process to the composition of deformational fluids. This suggests, that fluids likely traveled laterally for a significant distance before their involvement in clay mineralization. $^{40}Ar/^{39}Ar$-dating reveals that clay growth occurred during and after the main stages of orogenesis, indicating that metamorphic dehydration and fluid driving forces persisted for tens of millions of years following peak orogeny.

Several appendices support the main text of the Dissertation and two other studies are included. In a variety of geological settings, each appendix uses isotopic techniques to qualify the fluid regimes in deformed rock.

Appendix A, published in *Lithosphere* as Haines et al. (2016), uses isotopic studies of clay minerals to characterize and date fluid involvement in the extensional faults of the Basin and Range region. Using paired stable and radiogenic isotopic studies of authigenic clays, we identify meteoric fluid presence during Miocene to recent detachment faulting. Similarly to the mechanical implications surrounding low-angle thrust faulting, the presence of surface fluids in low-angle normal faults suggests that high fluid pressures are not likely to be the primary cause of slip on unfavorably oriented faults.

Appendix B explains the correction procedure used to determine the $^{40}Ar/^{9}Ar$-ages of some of the samples dated in this dissertation, supporting Chapters III and V.

Appendix C offers an exploratory study that complements work in the central Appalachians (Chapter V). Stable isotopic studies of a small subset of previously dated

fault and foreland shale rocks from the Southern Appalachians show varied fluid inputs. Based on H- and O-isotopic signatures, we determine that authigenic clays in the foreland shale unit formed in the presence of basinal fluids. Similarly to the Central Appalachian study, clays in two of the three fault structures formed from a mixture of metamorphic and surface-sourced fluids. In contrast, one of the major Southern Appalachian faults hosted primarily metamorphic fluids. This study suggests that fluid pathways in fold-thrust belts are not identical across mountain belts and that instead, certain structures may act as preferential fluid pathways for fluid escape from depth while others may not.

Appendix D discusses the results of an exploratory study of mercury isotopes as a fluids source tracer. Mercury isotopic fractionation patterns between fault rocks and host rocks in the San Andreas Fault (California) suggest that mercury does not preserve the isotopic composition of its source. Rather, the enrichment of light isotopes in the fault zone suggests that fractionation occurs during mercury mobilization and binding during fault processes. This offers interesting insights into the cycling of mercury through deep geologic reservoirs and its constituents, but limit its utility for geofluid source studies.

Chapter II. Meteoric fluid infiltration in the Argentine Precordillera fold-and-thrust belt: Evidence from H isotopic studies of neoformed clay minerals

Abstract

Fluids in the upper crust can affect the strength properties, composition, and mineralization of rock units, but the source(s) of these fluids and their transport during deformation are not well understood. Stable isotopic studies of clay-rich rocks, particularly newly formed illitic clays, shed light on the source of geofluids involved during faulting and folding. Hydrogen isotopic (δD) measurements of fault gouge and folded clay-rich sediments from the Argentine Precordillera show meteoric, surface-sourced fluid involvement during Miocene faulting. The δD composition of neoformed clay minerals is between -70‰ and -90‰ ± 2‰.The associated composition of fluids ranges from -57‰ to -72‰ ± 10‰, matching values for a surface-derived source. Regional Miocene meteoric fluid infiltrated down into the evolving fold-and- thrust belt, accumulated in basin sediments, and was subsequently expelled by the overriding rock units during late Miocene shortening. A systematic increase in δD signature with deformation age is preserved that matches regional climatic changes during late Miocene aridification, cooling, and glacial expansion.

Introduction

Fluid migration through Earth's crust plays a major role in the structural and chemical evolution of rock units. Fluids transport both heat and mass, resulting in the generation of secondary mineral species, including ores, veins, and, the focus of this

paper, clay minerals. Through studies of secondary minerals, it has been determined that fluids penetrate fault zones, as far down as the brittle-plastic transition (Kerrich et al., 1984; Gébelin et al., 2014; Menzies et al., 2014). Sibson (1994) was among the first to describe the dynamic interactions between faulting and fluid flow, noting that fault-related crustal stresses can cause fluid redistribution and, following on earlier work (Hubbert and Rubey, 1959; Byerlee, 1993; Muir-Wood and King, 1993), that fluids promote faulting by modifying the stress state of the crust. Additionally, stress reorganization during faulting can cause both dilatancy and overpressurization in the fault zone, allowing faults to act as conduits for fluids that are pumped through the crust during earthquake cycles (Muir-Wood and King, 1993; Sibson, 1994; Caine et al., 1996; Evans et al., 1997; Aydin, 2000; Faulkner et al., 2010).

Fluids moving through fault zones leave behind a record of their passage by chemically altering the host rock, yielding both transformed and neoformed minerals, including metasomatic mineral species, veins, and ores (Kerrich, 1986; Taylor, 1974; Micklethwaite et al., 2014). Many shallow-crustal faults develop clay-rich gouge during cataclastic deformation and mineralogical transformations associated with fluid flow (Engelder, 1974; Chester and Logan, 1987; Vrolijk and van der Pluijm, 1999; Haines and van der Pluijm, 2012). The chemical and stable isotopic composition of neoformed minerals can be used to probe the chemistry and origins of the geofluids from which they grew (Taylor, 1974).

Previous research in the area of geofluid sourcing has focused on secondary minerals in veins, ores, and fault rock for chemical and isotopic study. For example, secondary white mica in North American extensional fault systems has been the subject

of stable isotopic studies that aim to constrain the origin of fluids that are active deep in the crust (Fricke et al., 1992; Mulch et al., 2004; Gébelin et al., 2011, 2014; McFadden et al., 2015). These studies have indicated that meteoric fluids play a large role in detachment faults down to the brittle-plastic transition. In contrast, studies of clay minerals and veins formed in association with contractional fault systems have suggested input from deeper, metamorphic or magmatic fluids (Bradbury and Woodwell, 1987; Templeton et al., 1998; Uysal et al., 2006; Rossi and Rolland, 2014). This study aims to probe the origin of fluids in fold-and-thrust belts, which represent complex tectonic settings with protracted tectonic histories and complex geologies and deformation styles.

Fluids in fold-and-thrust belts

Hypotheses for geofluid sources and pathways in fold-and-thrust belts have implications for the dynamic evolution of mountain belts and fluid driving forces. End member sources include surface-derived fluids (meteoric, formational) at one end and deeply sourced (metamorphic) fluids at the other, as illustrated in Figure II.1. Fluid pathways and flow velocity depend on a variety of factors, including rock porosity and permeability, as well as thermal and pressure gradients (Ge and Garven, 1994; Lyubetskaya and Ague, 2009; Faulkner et al., 2010; Pollyea et al., 2015). Deformation in orogenic belts has the potential to increase permeability and porosity of the rock units through fracturing and faulting (Koons et al., 1998; Faulkner et al., 2010), while topography can provide a hydraulic head (Koons and Craw, 1991; Deming, 1994; Garven, 1995). Each of these processes has the effect of promoting flow of higher-elevation, hinterland-sourced meteoric water toward the foreland fold-and-thrust belt and foreland basin. Deep burial of rock during orogeny increases pressure and temperature,

resulting in prograde metamorphic dehydration reactions, which release associated metamorphic fluids (Bradbury and Woodwell, 1987; Ferry, 1988; Koons and Craw, 1991; Templeton et al., 1998). These increased pressure-temperature conditions instead promote the upward flow of deeply sourced geofluids, which migrate toward lower-pressure and lower-temperature conditions near the surface. Thrust sheet loading, sediment compaction, and pore space reduction may further promote the migration of fluids from the hinterland toward the foreland, expelling formational fluids, which may be either oceanic or meteoric in primary origin (Taylor, 1974; Sheppard, 1986; Oliver, 1986; Machel and Cavell, 1999).

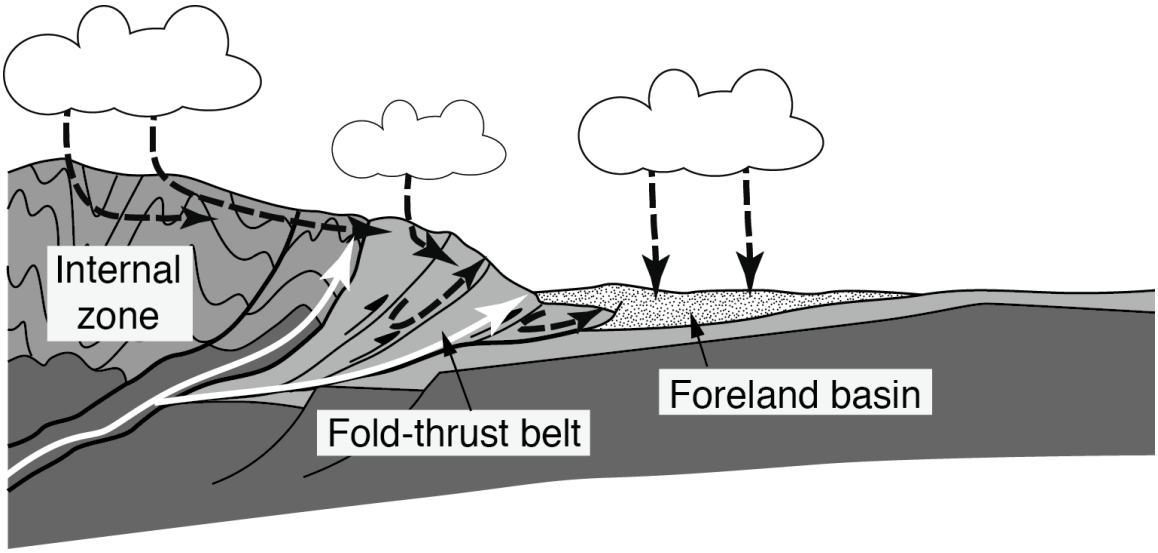

Figure II.1: Schematic representation of fluid sources and pathways in a fold-thrust belt. Solid white arrows represent deeply-sourced metamorphic fluids. Dashed black arrows represent surface-sourced meteoric fluids. Both high elevation precipitation and fold-thrust belt formational fluid may be the source of surface-derived fluids.

Different fluid source reservoirs have characteristic physical and chemical properties. Surface-sourced meteoric fluids are generally low in temperature and salinity, whereas deeply sourced metamorphic fluids are higher in temperature and salinity (Yardley and Bodnar, 2014). Formational fluids also tend to be higher in salinity, but

they have more moderate temperatures and are commonly associated with hydrocarbons, unlike meteoric and metamorphic fluids (Yardley and Bodnar, 2014). Notably, deeply sourced, high-temperature fluids, as opposed to surface-derived, low-temperature fluids, have distinct stable isotopic compositions of both hydrogen and oxygen (Taylor, 1974; Sheppard, 1986). Past geofluid studies have successfully exploited these differences, often using fluid inclusions to understand fluid chemistry and trapping temperature during fluid flow and vein formation (Evans and Battles, 1999; Barker et al., 2000; Lacroix et al., 2014). For example, Evans and Battles (1999) conducted a comprehensive study of fluid inclusion chemistry and oxygen isotopes in veins, revealing episodic fluid flow in the stratigraphy of the Appalachian foreland. In the Pyrenees, stable isotopic studies of pre-, syn-, and postorogenic veins also pointed to a complicated history of fluid origin and migration, with composition of fluids varying through time and space (Travé et al., 2007; Lacroix et al., 2014). In the Sevier fold- and-thrust belt of North America, vein oxygen isotope studies revealed fluid of mixed origins as well (Bebout et al., 2001; Anastasio et al., 2004; Vandeginste et al., 2012). Though these studies have elucidated a range of sources and pathways of orogenic fluids, they have limitations. First, veins are typically difficult to date, and their sequence of formation relies on interpretation of vein geometry and morphology. Similarly, the timing of fluid inclusions (whether primary or secondary) also depends on interpretations of vein morphology. Additionally, fluid inclusions can leak during deformation, potentially losing the primary chemical composition of fluids (e.g., Kendrick and Burnard, 2012). Last, the isotopic work of most studies relies on oxygen isotopes, which have been shown to buffer with host rock, losing potential far-field source signals and thus decreasing their general utility in determining

fluid sources (Ghisetti et al., 2001; Clauer et al., 2013; Rossi and Rolland, 2014).

Whereas oxygen is ubiquitous in earth materials, hydrogen is an uncommon element in most minerals, except clays and hydrocarbons, and thus it has the potential to reliably preserve far-traveled fluid source signatures. For example, Fitz-Diaz et al. (2014) used hydrogen isotopes in secondary clay minerals along with fluid inclusions and veins to study fluid sources in the Mexican fold-and-thrust belt, concluding that fluid source mixing played an important role during thrusting. Boles et al. (2015) examined the hydrogen composition of illitic clay in North Anatolian fault rocks, concluding that meteoric fluid infiltrated the crust during deformation. Additionally, Haines et al. (2016) looked at hydrogen isotopic signatures of neoformed clay minerals from low-angle normal faults in the Basin and Range and linked their composition to the downward infiltration of meteoric waters into the subsurface. These studies demonstrated that the hydrogen isotopic composition of neo- formed clay minerals can be a useful tool for geofluid studies in the upper crust.

Here, we present new hydrogen isotope results from neoformed clay minerals in the Precordillera fold-and-thrust belt of Argentina. This area was targeted for study due to the abundance of well-exposed clay-rich fault gouge and a well-constrained chronology of fault motion (e.g., Beer, 1990; Jordan et al., 1993; Alvarez-Marron et al., 2006; Allmendinger and Judge, 2014; Fosdick et al., 2015). Our results show that surface-derived fluids played a significant role in the evolution of this fold-and-thrust belt. We also use the results to examine the influence of changing climate or elevation on the isotopic composition of surface-sourced geofluids in the Precordillera during the late Miocene.

Geologic Setting

Central Andes

The southern Central Andes of Chile and Argentina are divided into several structural domains: the Coastal Cordillera, the Principal Cordillera, the Frontal Cordillera, the Precordillera, and the Sierras Pampeanas (Figure II.2a; Ramos, 1988; Ramos et al., 2002). The Coastal Cordillera is interpreted as a deformed and metamorphosed accretionary wedge that formed in the middle Paleozoic following the accretion of the Chilenia terrane (Herve et al., 1982, *in* Ramos, 1988). The Principal Cordillera is composed primarily of Mesozoic and Cenozoic volcanic units that make up the core zone of the Andes around 30°S. The Frontal Cordillera lies just to the east of the Principal Cordillera, consisting of faulted and deformed Paleozoic and Mesozoic rocks, including the Permian–Triassic Choiyoi Formation, which is composed primarily of granitoids and rhyolites (Kay et al., 1989). The Precordillera is a thin-skinned foreland fold-and-thrust belt that deforms Paleozoic to Cenozoic units and extends eastward from the Frontal Cordillera to the Bermejo Basin (Jordan et al., 1993; Ramos et al., 2002). Further east, the Sierras Pampeanas protrude from the foreland basin in a series of thick-skinned basement uplifts, which occur on steep, west-vergent thrusts (Ramos et al., 2002). The occurrence of oppositely verging, thin- and thick-skinned components of deformation in the foreland creates a triangle zone in the basin that is bounded on the east and west by thrust faults, between the two thrust fronts (Zapata and Allmendinger, 1996; von Gosen, 1997).

The lack of volcanic activity in the Main and Frontal Cordillera has been attributed to at-slab subduction of the Nazca plate below the South American plate, which

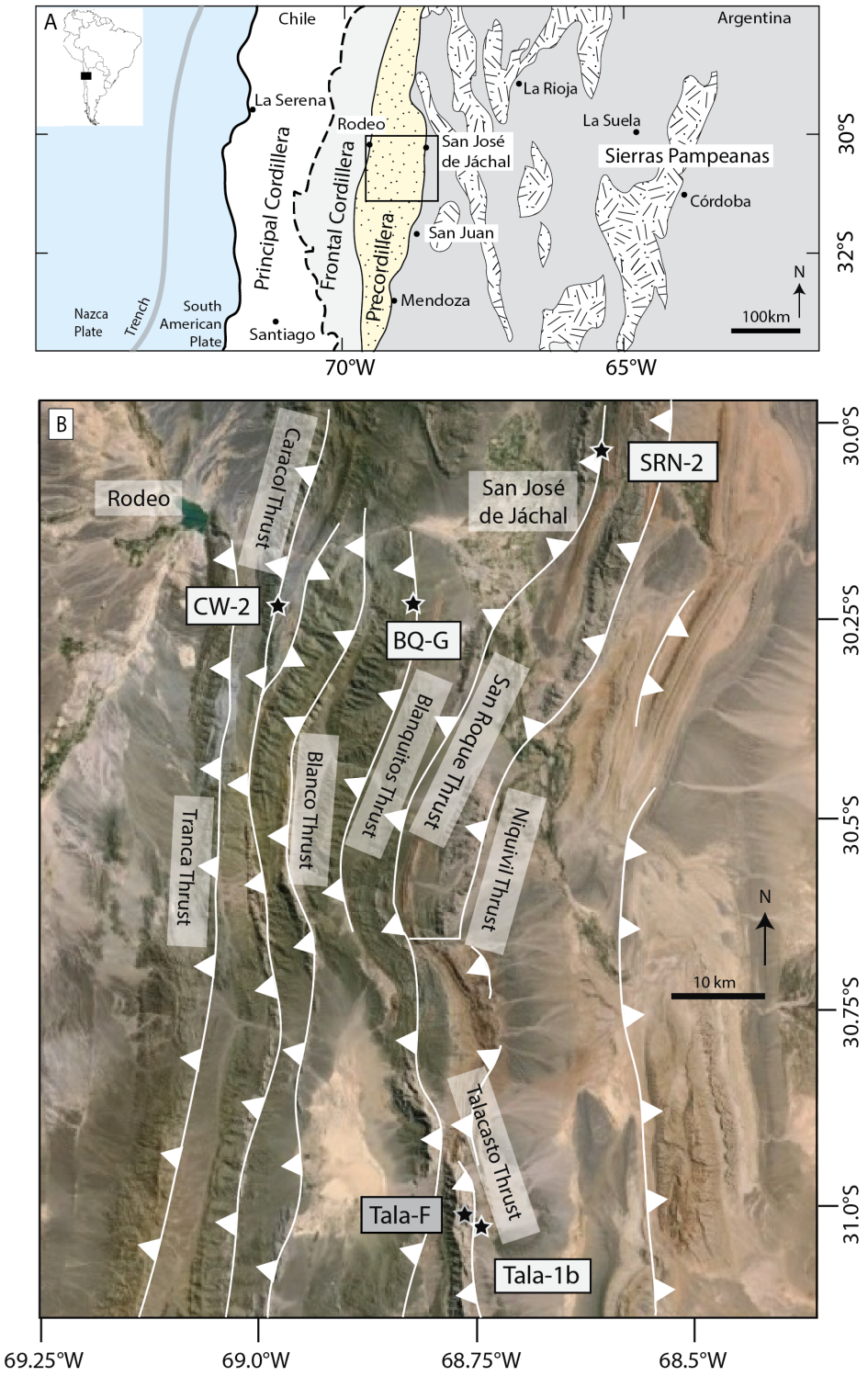

Figure II.2: a) Regional map of the south Central Andes (modified from Ramos, 2002) showing the positions of the main geologic domains. The study area is situated near the center of the regional map, indicated by the black bounding box. b) Google Earth image of the study area (bounding box in figure II.2a) showing major thrust structures and sample locations (after Ragona et al., 1995). Sample names in white boxes are fault gouge samples, whereas the sample name in the black box is from a folded clay-rich unit.

began around 20 Ma with the subduction of the Juan Fernández Ridge (Ramos et al., 2002). Neogene fault activity in the Precordillera fold-and-thrust belt also began around this time (Jordan et al., 1993; Fosdick et al., 2015). This is evidenced by sedimentation patterns in the Bermejo foreland as well as crosscutting and onlapping relationships, with earliest thrusting beginning at 21.6 ± 0.8 Ma and the majority of shortening occurring in the last 16 m.y. (Jordan et al., 1993). Recent thermochronologic studies have largely confirmed this timing of deformation (Fosdick et al., 2015). The well-constrained timing of deformation and extensive exposure of this fold-and-thrust belt make the Argentine Precordillera an ideal place in which to study orogenic fluid dynamics (Jordan et al., 1993; Alvarez-Marron et al., 2006).

Precordillera Fold-and-Thrust Belt

The Argentine Precordillera fold-and-thrust belt is located in the southern Central Andes of northwestern Argentina between ~28°S and 33°S latitude (Figure II.2b). Its protracted tectonic history began with a major period of rifting at ca. 600 Ma, which resulted in the formation of a carbonate platform bounded on its western edge by continental slope facies and oceanic crust (Ramos, 1988). The initiation of subduction during Ordovician and Early Devonian times is indicated by arc magmatism that is manifested in the western Sierras Pampeanas (Ramos, 1988). This volcanic arc was extinguished following the collision of the Chilenia terrane with the continental margin in the end-Devonian, which also caused the uplift and subaerial exposure of the carbonate platform units and the obducted ophiolitic units in an east-vergent thrust stack (Ramos, 1988; Alvarez-Marron et al., 2006). This episode of Paleozoic compression, which has been recognized and described by many authors (e.g., von Gosen, 1997; Alvarez-Marron

et al., 2006), created the structural setting upon which more recent deformation is superimposed.

Miocene to present deformation in the Pre-cordillera, referred to as the Andean orogeny, is responsible for the current configuration of the thrust sheets, mountain belts, and intervening basins (Ramos, 1988). Along the Jáchal River, the Precordillera is composed of six major thrust faults: From west to east, these are the Tranca, Caracol, Blanco, Blanquitos, San Roque, and Niquivil thrusts. These six faults place Paleozoic marine clastics and carbonates over Miocene–Pliocene continental sedimentary units (Allmendinger and Judge, 2014). The area can be divided into two regions based on the geology of the hanging-wall units. The two westernmost thrusts, Tranca and Caracol, expose the Ordovician Yerba Loca Formation, a deep-water turbidite horizon, whereas the eastern thrust sheets, Blanco, Blanquitos, and San Roque, bring Ordovician San Juan limestone and overlying formations to the surface (Allmendinger and Judge, 2014). Thrusting is thin skinned in character and dies out to the east, resulting in a series of synclines and anticlines that warp the stratigraphy of the Bermejo Basin. Though activation on some faults likely overlapped in time, thrusting generally proceeded from west to east, but also with instances of reactivation occurring in the Tranca and Caracol fault zones, as evidenced by thrusting within Tertiary-aged conglomerates that flank the valley walls (Jordan et al., 1993; Fosdick et al., 2015). The Talacasto thrust is situated just south of the well-studied Jáchal River section of the Precordillera, and it is exposed along Provincial Route 436. It too places Ordovician San Juan limestone on top of Neogene siliciclastics and is structurally correlated with the San Roque fault to the north. A recent stratigraphic study of both volcanic and detrital zircon ages and apatite (U-

Th)/He thermochronology from the bounding Talacasto basin sediments indicated that the age of thrusting in this area was coeval with major episodes of thrusting in the northern sections of the Precordillera (ca. 12–9 Ma; Levina et al., 2014; Fosdick et al., 2015). Incorporating this southern area in with the main transect provides regional context for fluid involvement in faulting. The frontal thrusts in the Precordillera are still actively deforming due to the continued subduction of the Nazca plate below the western margin of South America (Ramos et al., 2002). With fault activity extending from the present back through the early Miocene, δD signatures of neoformed clay minerals in the Precordilleran thrusts have the potential to record the sources of the fluids involved in thrusting and their potential evolution through time.

Methods

Sampling Strategy and Sample Preparation

Fault gouge samples in the Precordillera fold-and-thrust belt were collected in the San Juan Province of Argentina. Samples were taken from several major thrust faults in the area of the Jáchal River, along National Route 150 between Rodeo and San José de Jáchal and also along Provincial Route 436 between the junction of Route 40 and Route 149 (Table II.1; Figure II.2). At each fault outcrop, samples were taken from visibly distinct zones in the fault gouge as defined by variations in fault rock texture and color (Figure II.3). One sample, Tala-F, was taken from a folded clay-rich horizon within the San Juan Formation near the Talacasto thrust front.

Clay-rich rock samples were gently disaggregated by hand using an agate mortar and pestle in the clay laboratory at the University of Michigan. Disaggregated samples were suspended in deionized water and placed in a Branson 3510 ultrasonic bath for ~5

min to promote further disaggregation of clay mineral grains. Bulk-rock material was then washed with deionized water to remove salts, including halite and gypsum. The gouge samples were then separated by high-speed centrifugation according to Stoke's law in a Thermo Scientific CL-2 centrifuge. Gouge samples were divided into five clay-sized fractions (fine: <0.05 mm, medium-fine: 0.05–0.2 mm, medium: 0.2–0.5 mm, medium-coarse: 0.5–1 mm, and coarse: 1–2 mm).

Table II.1: Sample descriptions

Sample name	Structure	Latitude	Longitude	Description
CW-2	Caracol West Thrust	30.314°S	68.973°W	Green/grey fault gouge with significant siliciclastics
BQ-G	Blanquitos Thrust	30.305°S	68.821°W	Green, upper fault gouge, foliated clays
SRN-2	San Roque Thrust	30.144°S	68.609°W	White-yellow clay horizon below fault contact
Tala-1B	Talacasto Thrust	31.027°S	68.748°W	Green/red lower fault gouge
Tala-F	Chevron fold	31.025°S	68.753°W	Folded clay-rich layer in San Juan limestone

Size fractions were prepared for characterization by X-ray diffraction (XRD). First, we use oriented clay mounts for detailed clay mineral identification. Approximately 300 mg of each of the clay size fraction were suspended in 5 mL of deionized water and deposited onto glass slides using a dropper in accordance with the suspension method detailed by Moore and Reynolds (1997). Samples were left to dry in an oven at 50 °C for ~1–2 h. Powder mounts of size fractions were prepared for quantitative XRD polytype analysis using a top-loading, razor-tamping method to promote randomness of mineral orientation (Moore and Reynolds, 1997; Zhang et al., 2003).

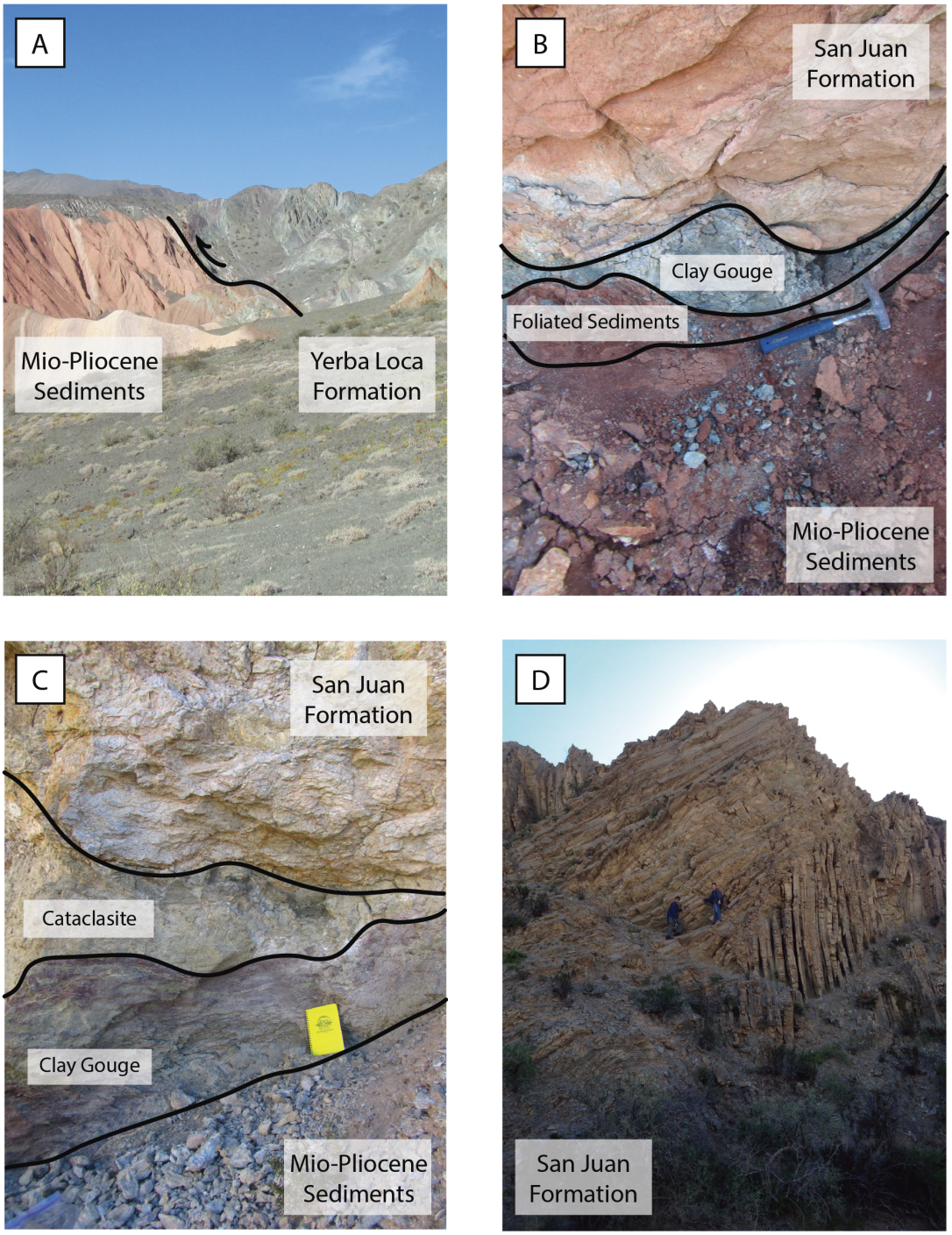

Figure II.3: Field photographs of sampled outcrops: a) View looking south along the Caracol Thrust (30.307°S, 68.973°W). The sharp color contrast between the sediments of the hanging wall and the footwall is evident. The Caracol Thrust places the Ordovician Yerba Loca formation on top of the Mio-Pliocene siliclastic basin sediments. b) Outcrop of the Blanquitos thrust fault (30.305°S, 68.821°W). The sample BQ-G is taken from the distinct green, clay-rich gouge zone between the San Juan formation in the hanging wall and the Mio-Pliocene sediments in the footwall. c) Outcrop of the Talacasto Thrust fault shows a damage zone consisting of an upper brecciated layer and a lower foliated, clay gouge. Sample Tala-1b was taken from this clay-rich layer (31.027°S, 68.748°W). d) Large chevron fold outcrop in the San Juan formation just west of the thrust fault. Sample Tala-F was taken from a clay-rich layer near the fold hinge at this outcrop (31.025°S, 68.753°W).

X-Ray Diffraction

Each oriented clay size fraction was scanned from 2° to 30° 2θ using a copper source Rigaku Ultima IV XRD at an accelerating voltage of 40 kV and lament current of 44 mA at a speed of 1°/min with a nickel-foil K-beta filter installed. Oriented slides increase the intensity of the clay mineral basal peaks, which are the most diagnostic for identifying clay phases. In order to identify expandable clay species (e.g., smectite and vermiculite), each oriented clay slide was placed in a glass desiccator with liquid ethylene glycol and heated in an oven at 50°C for at least 8 h prior to XRD analysis. Glycolated samples were then rescanned under the same X-ray conditions as described already. Random powder mounts were also scanned under the same machine conditions from 2° to 80° 2θ at a speed of 0.3°/min to obtain high-resolution X-ray patterns. High-resolution patterns allow for the quantification of clay mineral polytypes, which are key factors in identifying the distinction between detrital and neoformed clay species.

Clay Mineral and Polytype Quantification

Semiquantitative clay mineral proportions were calculated using the mineral intensity factor (MIF) method as outlined by Moore and Reynolds (1997). MIF uses the relative intensities of clay mineral basal reflections in order to quantify their relative proportions. For the calculation, peaks of each clay mineral species in a small 2θ range are chosen for comparison. We used the illite 002, chlorite 003, and, when present, smectite 003 peaks for our calculation. The integrated intensity of each peak is then compared to published mineral reference intensities (MRIs) of these peaks, which take into account mineral diffraction properties (Moore and Reynolds, 1997). Mineral proportion determinations are calculated by normalizing the intensities relative to an

internal reference peak, in our case illite 003. The accuracy of this calculation is approximately ±5% (Moore and Reynolds, 1997). Whereas the MIF method can be used to distinguish between different clay species (e.g., illite and chlorite) by comparing the different basal reflection peaks that are unique to each clay mineral, it cannot distinguish between different polytypes of the same clay species (e.g., $1M_d$ illite and $2M_1$ illite) that have the same basal peaks, which are key features in our application. All polytypes of illite have the same 00*l* reflections, but because of variable sheet stacking sequences, they have different nonbasal *hkl* peaks.

To determine the variation in illite polytypes between samples and size fractions, we used the end-member standard matching method described in Haines and van der Pluijm (2008). The $2M_1$ polytype of illite is a highly ordered, high-temperature mica polytype, which, in fault gouge, is detrital in origin, whereas the $1M_d$ polytype is a low temperature, disordered polytype that is authigenically formed (Vrolijk and van der Pluijm, 1999). Standards of monomineralic $2M_1$ illite (Owl Creek Muscovite) and $1M_d$ illite (Clay Mineral Society standard IMt-1 illite) were prepared, and random powder mounts of each were scanned using identical machine parameters along with the sample random powder mounts. Standard XRD patterns were input into a spreadsheet and mathematically mixed in various proportions to closely match the patterns of the samples (Figure II.4). Visual matching focuses on polytype specific (*hkl*) peaks and the shape of the XRD pattern baseline, minimizing match errors; the polytype quantification error is ±2%–3% (Haines and van der Pluijm, 2008).

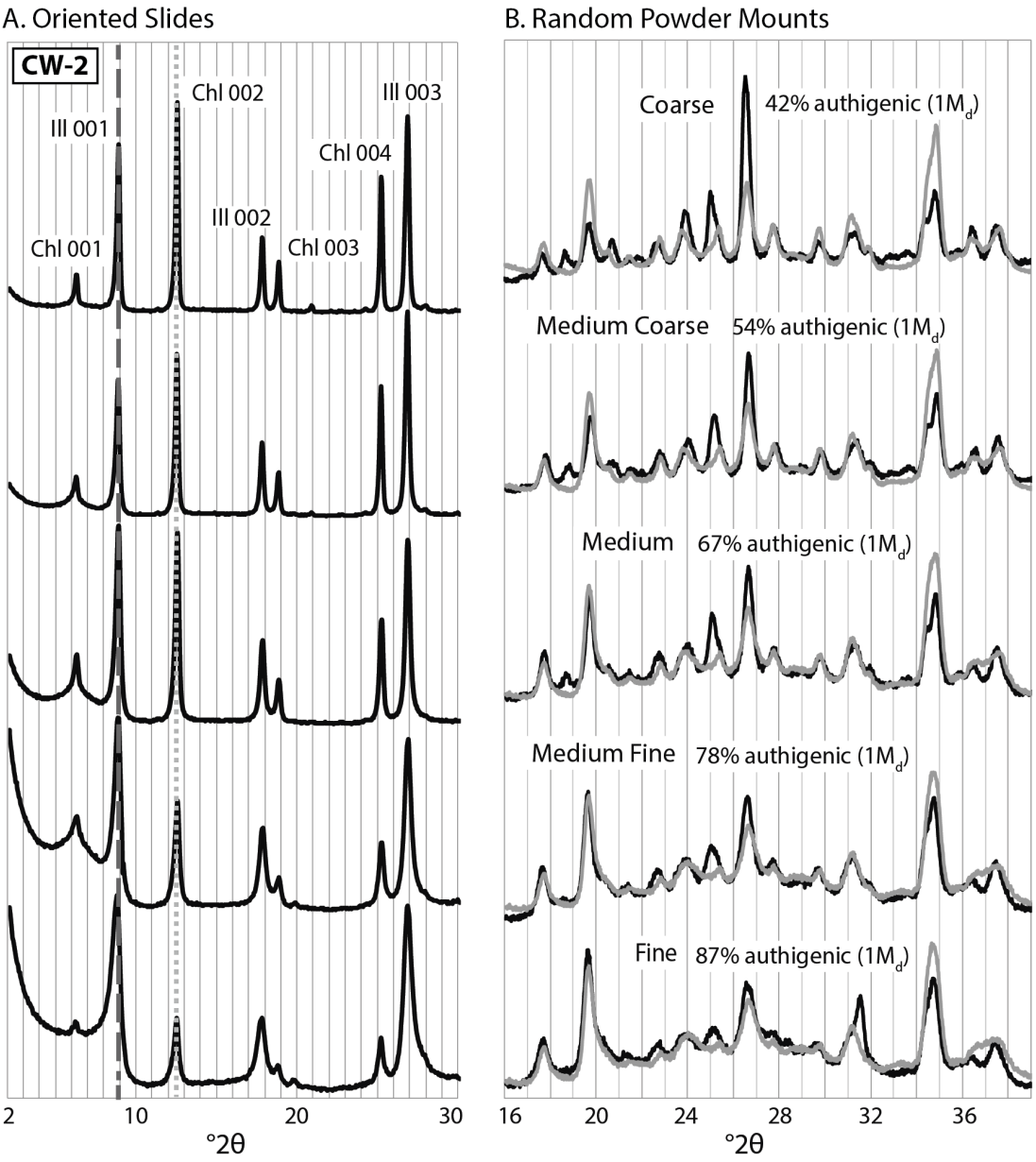

Figure II.4: Representative XRD patterns used for analysis of composition and clay polytype. The patterns show 5 size fractions from a single sample, CW-2, with coarse at the top and fine at the bottom of each column. a) Oriented slide XRD patterns from CW-2 sample show a trend of decreasing chlorite proportion (dark grey dashed line) in progressively finer fractions relative to an increasing proportion of illite (light grey dotted line). Note the changes in relative intensities of the two highlighted peaks between size fractions. b) Standards matching results for sample CW-2 from randomly-oriented powder mounts. The measured XRD patterns are shown in black, while the modeled patterns are shown in grey.

Authigenic ($1M_d$) Calculation

The proportion of authigenic $1M_d$ illite was calculated from the results of the MIF and standards matching analyses. Multiplying the proportion of total illite by the proportion of the illite of the $1M_d$ polytype gives the total proportion of $1M_d$ illite in each sample. Pairing the error of polytype quantification with that of δD measurements (~2‰ 3‰), we used a York-style regression to determine the δD composition of the $1M_d$ authigenic end-member illite (York, 1968). This regression method offers a more robust error analysis than standard regression analysis by incorporating individual errors in both polytype and δD quantifications.

Hydrogen Isotopic Analysis

Five samples that span the spatial and temporal deformational activity of the Precordillera (Figure II.2b) were divided into size fractions for hydrogen isotopic analysis. The Caracol West fault sample (CW-2) was taken from the western side of the study area (Figure II.2b), where continental slope facies of the Ordovician Yerba Loca formation are thrust atop Neogene basin sediments. Movement on this fault occurred between ca. 22–19 Ma and 16–13 Ma (Jordan et al., 1993). Samples from the Blanquitos (sample BQ-R) and San Roque thrusts (sample SRN-2) were taken in the eastern region of the Precordillera. These faults were active ca. 12–10 Ma and 11–2 Ma, respectively, and both place Ordovician San Juan limestone on top of Neogene siliciclastics (Ragona et al., 1995; Jordan et al., 1993; Allmendinger and Judge, 2014). The Talacasto thrust is structurally correlated with the San Roque thrust and outcrops ~100 km to the south of the San Roque sample outcrop. Two samples were collected, one sample from the fault zone (Tala-1b), as well as one sample from a clay-rich horizon within the hanging wall

<0.5 km from the fault outcrop (Tala-F). This fault also places Ordovician carbonates atop Neogene basin sediments and is thought to have been active from ca. 12 to 9 Ma (Levina et al., 2014). H-isotope measurements were completed on a Thermo Finnigan MAT 253 mass spectrometer coupled to a high-temperature conversion elemental analyzer (TC-EA) at the Biodiversität und Klima Forschungszentrum (BiK-F) Stable Isotope Laboratory in Frankfurt, Germany. Approximately 1 mg of each size fraction, one duplicate from each sample, and laboratory standards were individually encased in gold foil and kept overnight under vacuum at 200 °C. Samples were transferred to a zero-blank autosampler that was purged with helium gas to avoid rehydration with atmospheric moisture. The δD values are reported relative to standard mean ocean water (SMOW), with analytical error of approximately ±2‰.

York Regression

The mineralogical makeup of fault zones typically includes newly grown mineral phases and preexisting phases that are incorporated from the hanging wall and footwall through the process of cataclasis and entrainment. The latter, detrital grains, which are introduced into the fault zone due to fracturing of wall rock, generally dominate the coarse size fractions; authigenic phases, on the other hand, are generally smaller and thus dominate the finer clay grain-size fractions (Solum et al., 2005; Haines and van der Pluijm, 2012). To determine the δD value of fluids in fault zones from neoformed clays during fault activity, the authigenic minerals must be isolated from detrital minerals; however, due to the small size of clay minerals, this is physically impossible. Instead, we isolated the authigenic $1M_d$ illite signal using an end-member mixing calculation, similar to the procedures developed for illite dating (van der Pluijm et al., 2001). For each

sample, we plotted the δD value of each size fraction against the proportion of authigenic ($1M_d$) illite. Using a York regression, which takes into account the errors in both the δD measurements and polytype/mineral quantification (York, 1968), we obtained a best-fit line and envelope of error for multiple size fractions from a single sample (Figure II.5). From this analysis, we reliably extrapolated the δD value to that of 100% $1M_d$ illite and extrapolated the detrital composition from 0% $1M_d$ illite.

Fluid Isotopic Characterization

The temperature of fluid is a major factor in controlling the fractionation of hydrogen isotopes between minerals (here, illite) and fluids (e.g., Taylor, 1974; Chacko et al., 2001; Capuano, 1992). In contrast to oxygen isotopes, heavy hydrogen preferentially remains in the fluid, while light hydrogen is incorporated into illite crystals, yielding crystallites that exhibit more negative δD values than the fluid from which they grew (Savin and Lee, 1988; Capuano,1992). At lower temperatures, this pattern is more extreme, yielding illite crystals that are much more negative than their associated fluids, whereas at higher temperatures, fractionation is less pronounced, yielding crystals and fluids that are more similar in their hydrogen composition (Capuano, 1992). We used a range of temperatures for the formation of illite of 100°C to 150°C, which reflects the geologic constraints and limits of clay crystal ordering and stability. The growth of $1M_d$ illite in fault zones occurs in the temperature range of 100°C to ~180°C (Haines and van der Pluijm, 2012). Here, we used an upper boundary of 150°C based on a geothermal gradient of 25°C/km and estimates of sediment thickness and burial depths that did not exceed 5–6 km (Jordan et al., 2001). Additionally, a recent zircon helium thermochronologic study by Fosdick et al. (2015) concluded that temperatures in these

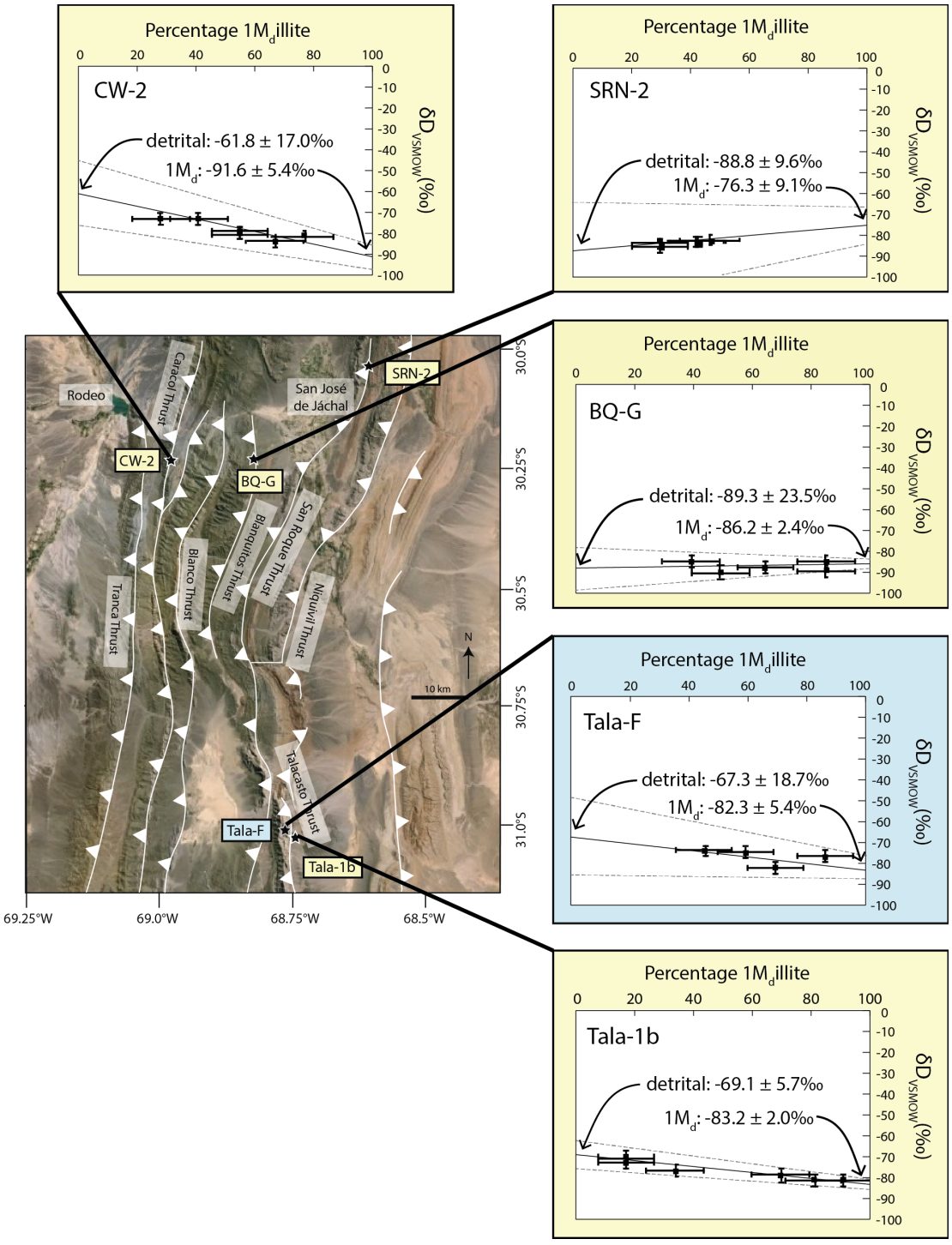

Figure II.5: York regression plots for the five samples showing the location of the samples in the study area. Plots with light grey backgrounds are fault gouge samples; plot with dark grey background is the clay-rich chevron fold sample. Percentage of authigenic $1M_d$ illite on the x-axis is plotted against the measured δD values of size fraction on the y-axis. For each sample, the solid black line is the best fit York regression line, and the dotted lines show the error envelope. Extrapolation to 100% $1M_d$ illite reveals the δD value of authigenic clay; extrapolation to 0% $1M_d$ illite reveals the δD value of detrital clay.

rock units of the Argentine Precordillera have not exceeded ~140°C since the Mesozoic, covering the period of Andean thrusting. Using published fractionation factors for illite (Capuano, 1992) and our temperature constraints, the composition of the mineralizing fluids was calculated. We used 125°C as an average temperature of authigenic illite formation in the Argentine Precordillera to determine the δD of mineralizing fluids.

Results

Mineralogy

Our XRD analysis of oriented samples revealed that each gouge sample contained several mineral phases, and that no size fraction was purely monomineralic. Each of the gouges contained both illite and chlorite as dominant clay phases. The mineralogy of each sample is summarized in Table II.2. Qualitative observations of the XRD spectra indicated that the ratio of chlorite to illite decreased greatly in progressively smaller size fractions (Figure II.4a), accompanied by an increase in the amount of smectite in some cases. The presence of at least trace amounts of smectite was ubiquitous, as shown by a peak at 5.2° 2q in the glycolated state, and this was especially prominent in smaller size fractions. Non-clay minerals were also present in the several of the size fractions. Quartz appeared in each gouge sample, with the highest relative abundance in coarse fractions and lowest abundance in fine fractions. Feldspar was present in three of the samples, including Tala-F, BQ-G, and SRN-2. Similar to quartz, feldspar was more abundant in the coarse fractions and tended not to be present in the finest fractions. Calcite was a common phase in many of the gouges as well, appearing in many size fractions of the SRN-2 and Tala-F samples. The presence or absence of calcite did not follow any abundance trends with size fraction. Gypsum was the dominant phase in a single size

fraction (Tala-F, fine), which was not used for isotopic analysis due to the lack of sufficient clay minerals.

Clay Mineral Quantification

The results of both the MIF and end-member standards matching quantification methods are summarized in Table II.3, along with the calculated total proportion of neomineralized ($1M_d$) illite and detrital ($2M_1$) illite. For each sample, the proportion of $1M_d$ illite increased in smaller size fractions as the amount of detrital phases decreased (Figure II.4b). Only one sample (SRN-2) contained a significant amount of smectite, which dominated the smaller size fractions. As a result, this sample resulted in a larger error after York regression analysis.

Table II.2: Sample Mineralogy									
Sample name	Size fraction	Chlorite	Illite	Polytype	Smectite	Quartz	Feldspar	Calcite	Gypsum
CW-2	1.0-2.0 µm	x	x	2M1/1Md	trace	x			
	0.5-1.0 µm	x	x	2M1/1Md	trace	trace			
	0.2-0.5 µm	x	x	2M1/1Md	trace				
	0.05-0.2 µm	x	x	2M1/1Md	x				
	<0.05 µm	x	x	2M1/1Md	x				
BQ-G	1.0-2.0 µm	x	x	2M1/1Md	x	x			
	0.5-1.0 µm	x	x	2M1/1Md	x	x			
	0.2-0.5 µm	x	x	2M1/1Md	x	x			
	0.05-0.2 µm	x	x	2M1/1Md	x	trace			
	<0.05 µm	x	x	1Md	x				
SRN-2	1.0-2.0 µm	x	x	2M1/1Md	x	x			
	0.5-1.0 µm	x	x	2M1/1Md	x	x			
	0.2-0.5 µm	x	x	2M1/1Md	x	x			
	0.05-0.2 µm	x	x	1Md	x	trace			
	<0.05 µm	x	trace	1Md	x				
Tala-1B	1.0-2.0 µm	x	x	2M1/1Md		x			
	0.5-1.0 µm	x	x	2M1/1Md		trace			
	0.2-0.5 µm	x	x	2M1/1Md					
	0.05-0.2 µm	x	x	2M1/1Md	trace				
	<0.05 µm	x	x	1Md	trace				
Tala-F	1.0-2.0 µm	x	x	2M1/1Md		x	x	x	
	0.5-1.0 µm	x	x	2M1/1Md	x	x	trace	x	
	0.2-0.5 µm	x	x	2M1/1Md	x	x		x	
	0.05-0.2 µm	trace	x	1Md	trace	trace		x	
	<0.05 µm							x	x

Table II.3: Illite quantification				
Sample name	Size fraction	% Illite (±5%)	Fraction $1M_d$ polytype (±0.02)	Total % $1M_d$ illite (±10%)
CW-2	1.0-2.0 μm	79	0.42	33
	0.5-1.0 μm	81	0.54	44
	0.2-0.5 μm	84	0.67	56
	0.05-0.2 μm	89	0.78	69
	<0.05 μm	90	0.83	75
BQ-G	1.0-2.0 μm	81	0.48	39
	0.5-1.0 μm	73	0.67	49
	0.2-0.5 μm	75	0.85	64
	0.05-0.2 μm	87	0.98	85
	<0.05 μm	85	1	85
SRN-2	1.0-2.0 μm	71	0.42	30
	0.5-1.0 μm	62	0.48	30
	0.2-0.5 μm	59	0.72	42
	0.05-0.2 μm	57	0.83	47
	<0.05 μm	43	1	43
Tala-1B	1.0-2.0 μm	85	0.27	23
	0.5-1.0 μm	85	0.42	36
	0.2-0.5 μm	87	0.82	71
	0.05-0.2 μm	90	0.94	85
	<0.05 μm	91	1	91
Tala-F	1.0-2.0 μm	89	50	45
	0.5-1.0 μm	90	65	59
	0.2-0.5 μm	89	78	69
	0.05-0.2 μm	96	90	86

Hydrogen Isotopic Composition of Illite and Mineralizing Fluids

Hydrogen isotopes were measured for five samples totaling 24 size fractions. The δD values are reported relative to SMOW and range from -70‰ to -90‰ ± 2‰ (Table 4). The hydrogen isotope values of each size fraction represent a composite value that is equal to the total amount of hydrogen contained in all the hydrous phases, including detrital chlorite, detrital illite, authigenic illite, and authigenic smectite, which varied in each size fraction for a single fault. The raw values reported in Table 4 here were used in the York regression to extrapolate the hydrogen isotopic composition of 1Md and 2M1 illite in each sample (Table 5). Along the Jáchal River transect, the Caracol fault (ca. 16–13 Ma) contained authigenic illite with a δD of -91.6‰ ± 5.4‰, the Blanquitos fault (ca. 12–10 Ma) contained authigenic illite with a δD of -86.2‰ ± 2.4‰, and the San Roque

fault (ca. 11–2 Ma) contained authigenic illite with a δD of -76.3‰ ± 9.1‰. Further to the south in the Talacasto area, the fault contained authigenic illite with a δD of -82.3‰ ± 5.4‰, while the folded shale showed a δD of -83.2‰ ± 2.0‰.

Table II.4: δD measurements

Sample name	Size fraction	δD_{VSMOW} (±2‰)	(duplicate)
CW-2	1.0-2.0 μm	-73	
	0.5-1.0 μm	-73	
	0.2-0.5 μm	-79	-80
	0.05-0.2 μm	-84	
	<0.05 μm	-81	
BQ-G	1.0-2.0 μm	-85	
	0.5-1.0 μm	-90	
	0.2-0.5 μm	-88	
	0.05-0.2 μm	-85	-85
	<0.05 μm	-89	
SRN-2	1.0-2.0 μm	-85	
	0.5-1.0 μm	-85	-86
	0.2-0.5 μm	-84	
	0.05-0.2 μm	-83	
	<0.05 μm	-84	
Tala-1B	1.0-2.0 μm	-70	-73
	0.5-1.0 μm	-77	
	0.2-0.5 μm	-79	
	0.05-0.2 μm	-81	
	<0.05 μm	-81	
Tala-F	1.0-2.0 μm	-74	-74
	0.5-1.0 μm	-75	
	0.2-0.5 μm	-82	
	0.05-0.2 μm	-77	

Using the results from our mixing model, we determined the δD value of fluids in Precordillera thrust fault zones during fault activity and authigenic mineral growth (Table 6). We calculated the δD value of the mineralizing fluid over a temperature range of 100° to 150°C (Table 6). Results range from the isotopically lightest sample, CW-2 (-59‰ to -85‰), to the heaviest sample, SRN-2 (-40‰ to -73‰).

Table II.5: York regression results				
Sample name	δD of 1Md illite	Error	δD of detrital clay	Error
CW-2	-91.6 ‰	5.4 ‰	-61.8 ‰	17.0 ‰
BQ-G	-86.2 ‰	2.4 ‰	-88.8 ‰	9.6 ‰
SRN-2	-76.3 ‰	9.1 ‰	-89.3 ‰	23.5 ‰
Tala-1B	-83.2 ‰	2.0 ‰	-69.1 ‰	5.7 ‰
Tala-F	-82.3 ‰	5.4 ‰	-67.3 ‰	18.7 ‰

Table II.6: δD fluid calculations					
Sample name	δD illite	Error	δD fluid (100°C)	δD fluid (125°C)	δD fluid (150°C)
CW-2	-91.6‰	5.4‰	-59‰	-72‰	-85‰
BQ-G	-86.2‰	2.4‰	-57‰	-67‰	-76‰
SRN-2	-76.3‰	9.1‰	-40‰	-57‰	-73‰
Tala-1B	-83.2‰	2.0‰	-54‰	-64‰	-73‰
Tala-F	-82.3‰	5.4‰	-50‰	-63‰	-75‰

Discussion

Our results constrain interpretations of the fluid-mediated processes involved in fault rock generation and geofluid sources. The extrapolation of York regressions and fractionation values gives fluid source δD values—extrapolation to 100% authigenic clay reveals information about the nature of deformational fluid, while extrapolation to 100% detrital clay reveals information about the nature of host rock grains and their associated fluid source(s). The δD signatures of authigenic $1M_d$ illite fall within a relatively narrow range (-76.3‰ ± 9.1‰ to -91.6‰ ± 5.4‰), whereas the detrital δD values show two distinct signatures. Three samples, CW-2, Tala- 1b, and Tala-F, have detrital δD signatures that range from -61.8‰ ± 17.0‰ to -69.1‰ ± 5.7‰; two samples, BQ-G and SRN-2, have detrital δD signatures that are -88.8‰ ± 9.6‰ and -89.3‰ ± 23.5‰, respectively. Our interpretation for these authigenic and detrital clays is discussed next.

δD Composition of Authigenic and Detrital Clay Phases

The oldest fault gouge sample, CW-2 (ca. 16–13 Ma), yields a regression line that shows a distinct trend in δD with grain size (Figure II.5). This sample comes from the

western side of the study area, where hanging-wall units are composed primarily of deep-water mudstones. These sediments likely contributed a significant amount of older (Paleozoic) detrital chlorite to the fault zone (von Gosen, 1997). Similarly, the southern Talacasto fault and fold samples (Tala-1b and Tala-F, ca. 12–9 Ma) show a trend that relates the δD values and percentage of detrital material, indicating input of detrital clays from an older source. The -61.8‰ to –69.1‰ range is consistent with metamorphic chlorite signatures (Taylor, 1974).

The δD values for samples BQ-G (ca. 12–10 Ma) and SRN-2 (ca. 10–2 Ma) do not follow a distinct trend. For these younger two faults, which were sampled in the eastern region of the Jáchal River transect, regression lines are nearly horizontal, reflecting homogeneity of δD values across size fractions within each sample. This uniformity can be interpreted in two ways. First, this could indicate an overall resetting of detrital δD values due to the exchange of hydrogen with the fault fluid during authigenic clay growth. However, it is unlikely that these fault gouge samples reached temperatures well over 150 °C, based on thermochronologic studies of these units (Fosdick et al., 2015). The likely explanation for homogenous δD values is multiple sources of detrital clay minerals, a process we describe in the following paragraph.

For the BQ-G and SRN-2 samples, we propose two distinct detrital mineral sources. The first, metamorphic chlorite, would contribute a portion of hydrogen to the isotopic signature that falls within the range of values for the CW-2, Tala-1b, and Tala-F samples. The second source, modern soil smectite, would also contribute to the hydrogen isotopic signature. Though isotopic studies of soil smectite in this area have not been done, a rough estimation of expected δD composition of smectite using the smectite

water fractionation factor (Capuano, 1992) can be obtained. From the mean annual temperature (16.5 °C), we predict a fractionation of -61.5‰ between smectite and water. Given the average δD of -37.5‰ for modern meteoric fluids calculated from reported δD measurements taken at Mendoza, Argentina, La Serena, Chile, and La Suela, Argentina, the three closest Global Network of Isotopes in Precipitation (GNIP) stations (IAEA/WMO, 2016), we predict that smectite δD values would be around -99‰. Therefore, the presence of significant smectite in these samples would drive the δD values toward the more negative end of the δD spectrum, obscuring the signature of the Paleozoic detrital metamorphic chlorite, as we observe.

δD Composition of Mineralizing Fluids

We calculated the approximate fluid δD composition for crystallization temperatures of 125°C, the median value for our range of possible temperatures. The δD fluid values fall in a range between -57‰ and -72‰ across all five of the samples. The relative homogeneity of fluid isotopic signatures from authigenic clays indicates a common fluid source across the region. The negative δD values of the fluid require significant input from a meteoric source, since no other reservoir has δD values as depleted in heavy isotopes (Figure II.6). Given that authigenic illite δD values are comparable and of meteoric origin, we propose that fluids involved in deformation are surface sourced fluids, derived in part from the Miocene foreland basin sediments and in part from infiltrating meteoric fluids. Formation fluids in foreland basins may be either shallow marine or meteoric (Taylor, 1974; Sheppard, 1986). In the case of the Argentine Precordillera, stratigraphic studies indicated that the region was not at sea level during deposition (Jordan et al., 2001), so it is likely that formation fluids in the foreland

sediments of the Bermejo Basin represent a composite of the Miocene meteoric water that fell both on the basin itself and on the higher-elevation ranges of the Precordillera to the west (Hoke et al., 2014). We surmise that the meteoric-derived formational fluids contained within the basin sediments were forced out of the sediments due to pore space compaction associated with compression and faulting in the Precordillera thrust belt. Formational fluids were then incorporated along with actively infiltrating meteoric fluids into the fault zone, imparting their δD signatures to the authigenic $1M_d$ illite. Because the system involved multiple fluid sources integrated through time scales of millions of years, we do not speculate on specific interpretations of each numerical value. Instead, our interpretation focuses on large-scale temporal trends throughout the time period of Miocene faulting in the Precordillera in order to constrain the processes that drove the changes in δD signatures of meteoric-sourced deformational fluids.

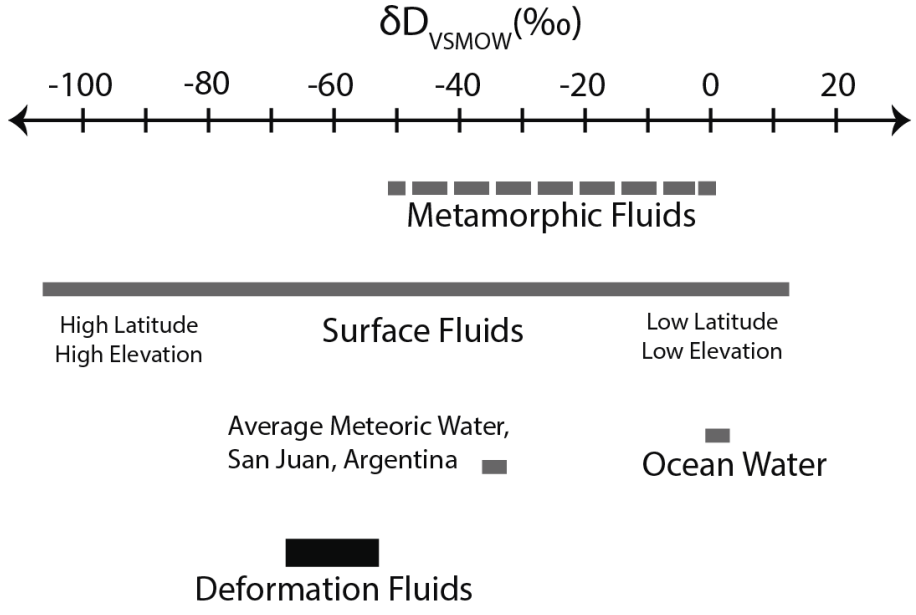

Figure II.6: δD scale showing the composition of surface-sourced (solid grey bars) and deeply-sourced, metamorphic fluid reservoirs (dashed grey bar) (Sheppard, 1986) compared to the deformation fluid signatures measured in this study (heavy black bar). For reference, the average δD composition of meteoric fluid in the study area is included and ocean water (SMOW) are both plotted as grey bars.

Drivers of Change: Climate or Tectonics

Despite the differences in hanging-wall rock composition and location in the study area, all fault and fold samples point to meteoric-derived, surface-sourced fluids. Since the isotopic composition of meteoric waters can be modified by both climatic and tectonic processes, the δD values preserved in fault gouge clays and, more specifically, the trends observed through time in these δD values will reflect the influence of these processes. There are two possible scenarios for major drivers of change in the isotopic composition of meteoric-derived deformational fluids and associated neoformed clay minerals: (1) the gradual uplift of the drainage area due to tectonic shortening of the Precordillera fold-and-thrust belt, and (2) the cooling and aridification of climate during the Miocene in this region of South America. The fractionation of stable hydrogen (and oxygen) isotopes in atmospheric H_2O by these processes would have opposite and competing effects on the composition of meteoric fluids.

For scenario 1 (uplift), the Rayleigh distillation of rainwater as it moves up in elevation causes progressively higher-elevation sites to receive more negative isotopic precipitation (Gat, 1996). The late Miocene in central South America was associated with the progressive uplift of the Precordillera fold-and-thrust belt and subsequent uplift of the Sierras Pampeanas (Sobel and Strecker, 2003; Hoke et al., 2014). The surface uplift of these ranges, therefore, would be associated with progressive evolution of meteoric water toward more negative stable isotopic values through time. In scenario 2 (climate), there would be the opposite effect. The late Miocene was a time of general cooling and aridification in the region of the Precordillera (Flower and Kennett, 1994; Cerling et al., 1997). Cooling of the climate was associated with the growth of the Antarctic ice sheet,

which sequestered negative hydrogen isotopes in the ice sheet and progressively enriched the oceanic reservoirs in heavy isotopes (Zachos et al., 2001). This would make precipitation sourced from the oceans become less negative through time. Alternatively and/or additionally, the trend toward heavy isotopic enrichment with time may have been a result of aridification, where basinal waters become evaporatively enriched in heavy isotopes in arid climates (Sheppard, 1986). Studies have shown that the late Miocene in the south Central Andes may have experienced such climatic aridification (Flower and Kennett, 1994; Cerling et al., 1997; Jordan et al., 2001). Regardless, both of these scenarios offer a trend driven by changing climate patterns that caused a shift in the stable isotopic values from more negative (light) toward less negative (heavy) values. Because these scenarios have opposite effects on the composition of stable isotopes in meteoric and, therefore, deformational fluids, our data set can distinguish between these two competing processes of isotopic fractionation.

To test the two scenarios, we plotted the δD_{fluid} values for each fault sample along with published estimates of fault activity (Figure II.7), where ages are from Jordan et al. (2001), Allmendinger and Judge (2014), and Levina et al. (2014). This plot reveals that progressively younger faults from the Jáchal River transect have meteoric fluid signatures that have progressively heavier δD signatures. This general trend in the δD value of meteoric fault fluids, being less negative through time, is consistent with a climate dominated signal, as described in scenario 2. Notably, we do not observe a decrease in the δD values as predicted by scenario 1, indicating that any topographic-related (uplift) isotopic signal is insignificant. We note that the combined effect of these two scenarios would have a dampening effect on the intensity of the changes observed in our isotopic

δD values, such that the climate signal dominating the fault fluid signature may be even more subdued than full isotopic trends in Miocene precipitation.

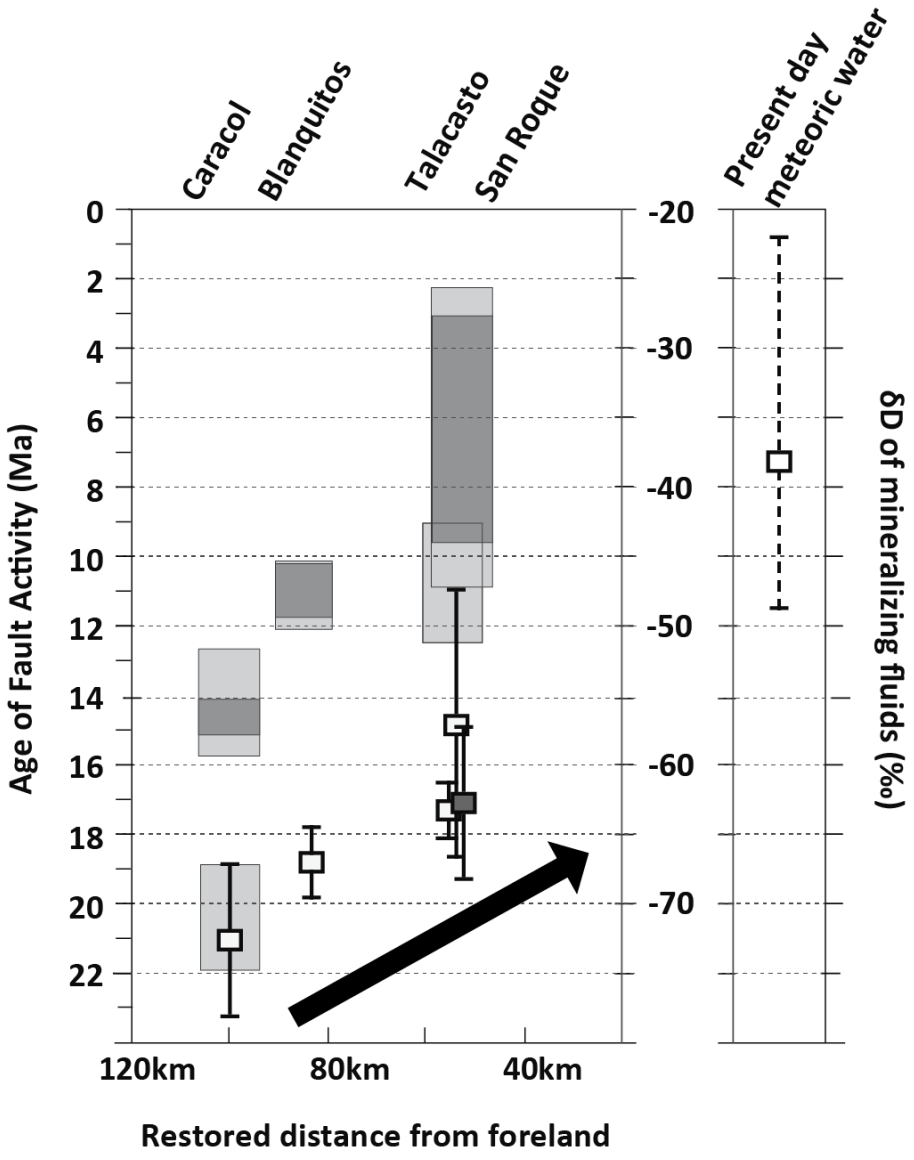

Figure II.7: Plot of deformation age range (adapted from Allmendinger and Judge, 2014) and δD of mineralizing fluids across 4 deformation zones of the Argentine Precordillera, compared with modern day meteoric water samples from three nearby GNIP stations (Mendoza, Argentina, La Serena, Chile, and La Suela, Argentina—see figure II.2 for locations). For the age of deformation, dark grey boxes represent the most likely period of deformational activity; light grey boxes represent the time period of possible activity. Boxes with error bars represent corresponding δD content of deformation-related fluids. As in figure II.2, light grey boxes represent fault gouge samples and the dark grey box represents the clay-rich folded sediment sample (Tala-F). The rightmost (white) box shows today's average meteoric δD value, while dotted lines show the range of the inner 50% of all modern meteoric measurements in the region. The observed trend is highlighted with a bold, black arrow.

Other stable isotopic studies in the Central Andes have revealed similar patterns of isotopic enrichment. Kleinert and Strecker (2001) observed a progressive increase in $\delta^{18}O$ and $\delta^{13}C$ of paleosol carbonates from 12 Ma to present, attributing the trend to increased aridity and evaporation in the Santa Maria Basin of the Northern Sierras Pampeanas (northeast of our study area), interpreted in part to be a consequence of uplifting mountain ranges and developing rain-shadow effects during the middle Miocene. Similarly, Latorre et al. (1997) analyzed paleosol carbonates from a stratigraphic section close to those of Kleinert and Strecker (2001) and observed a positive shift in $\delta^{18}O$ starting around 9 Ma, which they too attributed to changing climatic patterns and increased aridity. A more recent study of paleosol carbonate stable isotopes similarly documented increasing $\delta^{18}O$ values since ca. 7.14 Ma, corresponding to an ash bed near the bottom of the studied stratigraphic section (Hynek et al., 2012).

Today's meteoric fluid composition in the Precordillera is monitored by nearby sites in the GNIP. Three of the closest monitoring sites, Mendoza, Argentina, La Serena, Chile, and La Suela, Argentina (Figure II.2), show an average meteoric δD fluid of -37.5‰ (n = 130), with 50% of δD measurements falling within the range of -23‰ to -49‰ (Figure II.7; IAEA/WMO, 2016). These three monitoring locations at relatively low-altitude sites may be biased toward heavy isotopes relative to the Central Andes region as a whole. However, recent studies of stable isotopes in precipitation and river waters around Mendoza, Argentina, confirm that the stable isotopic composition of surface waters correlates with the average elevation of the drainage area (Hoke et al., 2009, 2013). Our measured values of δD in progressively younger faults follow the trend of increasing heavy hydrogen of Miocene meteoric waters (-72‰ to -58‰), as preserved

in clays of the Precordillera, providing evidence for a dominant climatic driver on evolving δD signatures of geofluids in this part of the Central Andean fold-and-thrust belt.

Conclusions

The isotopic compositions of authigenic clay minerals in fault gouge from the southern Central Andes reflect a geofluid source that is dominated by surface-derived fluids. This contrasts with the hypothesis that metamorphic fluids characterize contractional environments (e.g., Oliver, 1986; Bradbury and Woodwell, 1987; Templeton et al., 1998; Uysal et al., 2006; Rossi and Rolland, 2014). Though we cannot rule out some input of metamorphic fluids, the infiltration of greater volumes of meteoric fluids and the incorporation of meteoric-derived formational fluids were the primary fluid sources during contractional faulting in the Precordillera fold-and-thrust belt. The δD signatures of the geofluids are not so negative as to support a solely high-elevation meteoric origin; rather, we interpret them as a mixture of meteoric fluids that fell on the Miocene fold-and-thrust belt and in the co-evolving foreland basin. Second, the span in ages of faulting and the associated mineral neocrystallization preserve the changing characteristics of the meteoric-sourced fluid through time. The shift in δD of geofluids from more negative to less negative values over the time span of the late Miocene (ca. 16–2 Ma) reflects a change in regional climate (Flower and Kennett, 1994; Cerling et al., 1997) rather than a change in elevation (Sobel and Strecker, 2003; Hoke et al., 2014) of the Andean range. Late Miocene cooling and aridification support the observed increasing δD signature of fault rock fluids with time; indeed, fault rocks are sensitive recorders of climatic conditions in the area.

This study of neoformed clay in fault rocks shows that δD signatures can be used to determine the source and pathways of geofluids during deformation. The dominance of meteoric fluids requires infiltration during contractional tectonics, with, at best, minor metamorphic fluid input. Additionally, stable isotopes of fault rock in this and other fold-and-thrust belts may be used to constrain regional climatic conditions.

Acknowledgements

This chapter was published in the journal *Lithosphere* with co-authorship of Ben van der Pluijm. We thank Laura Giambiagi and her students at Instituto Argentino de Nivología, Glaciología y Ciencias Ambientales (IANIGLA) in Mendoza, Argentina, as well as Chris Banner, for their help with field logistics. We also thank Rick Allmendinger for his help in identifying outcrop locations in the Precordillera. We are grateful to Andreas Mulch at the BiK-F, Sencken- berg University, Frankfurt, Germany, for H isotopic analyses. We also thank Zhongrui Li at the University of Michigan Electron Microbeam Analysis Laboratory (EMAL) for assistance with X-ray diffraction. Furthermore, we wish to thank two anonymous reviewers, whose thorough and constructive comments greatly improved both the clarity and scope of the manuscript. This work was supported by Turner Graduate Research Grants and a Rackham Graduate Research Grant (both University of Michigan) to Lynch and partially supported by National Science Foundation grant EAR-1118704 to van der Pluijm.

Chapter III. Surface fluids in the evolving Sevier fold-thrust belt of ID-WY indicated by hydrogen isotopes in dated, authigenic clay minerals

Abstract

Using the hydrogen isotopic composition (δD) and 40Ar/39Ar geochronology of neomineralized clay minerals in deformed units of the Sevier belt, we recognize the primary involvement of surface-sourced fluids during Cretaceous-Paleogene mountain building events. δD values of authigenic clays range from -78.8±1.7‰ to -97.2±3.2‰. Given temperature constraints, we calculate δD values of mineralizing fluids as ~ -63 to -96‰, which fall within the range of δD values of Cretaceous-Paleogene surface waters in the region. The potential infiltration and presence of surface fluids at depths of several kilometers during deformation implies that pore spaces and fractures acted as conduits for surface water. This is in contrast to the hypothesis that the release of overpressured metamorphic fluids dominates during fold-thrust belt formation. As a result of shortening and tectonic uplift, fluid flows through basin sediments toward the foreland basin as meteoric waters recharge sediments at the basin margins. This study shows that stable isotopic compositions of low-temperature, shallow crustal clay minerals are robust and may be used to probe the origin and composition of ancient surface waters.

Introduction

Fluids in upper crustal rocks play a fundamental role in the evolution of the continental crust by changing the physical and chemical characteristics of rock units

involved in deformation. Fluids promote chemical reactions, which include in the formation of post-depositional minerals (e.g., Haines and van der Pluijm, 2012; Clauer et al., 2013). Additionally, fluids in the crust can modify the stress state that promotes deformational processes. Determining the nature and source of these fluids has fundamental implications for understanding orogenic processes, but remains a challenge. Studies of the hydrologic regimes of upper crustal faults have provided multiple hypotheses regarding the migration of fluids in faults. Several studies suggest that deeply-sourced metamorphic, magmatic, and mantle-derived fluids use through-going crustal-scale faults as pathways for escape to the Earth's surface (e.g., Kennedy et al., 1997; Haney et al., 2005). Others have proposed that faults act as conduits for downward fluid migration, allowing surface water to penetrate the crust down to the brittle-ductile transition (e.g., Mulch et al., 2004; Haines et al., 2016). We can ascribe the balance of these two end-member hypotheses to two main fluid movement drivers. The first is different crustal stress regimes; for example, in extensional environments surface-fluids are drawn down into the crust (Muir-Wood and King, 1993; Sibson, 1994; Person et al. 2007; Haines et al., 2016), whereas in compressional systems fluids are squeezed out of the crust, migrating towards areas of lower stress (Oliver, 1986; Koons and Craw, 1991; Muir-Wood and King, 1993). In regions where crustal fluids are at hydrostatic pressures, circulation and migration are dependent on temporary or short term regional temperature and pressure gradients, whereas in regions where fluids are hydrostatically overpressured, fluid migration is typically unidirectional (Walther and Wood, 1984). Building upon this concept, it follows that the extent of the connectivity between crustal levels will also have an effect on the types of fluids involved in faulting. Steeply dipping, crustal faults are

more likely to involve overpressured, deeply-sourced fluids, whereas shallowly dipping faults are more likely to tap upper-crustal reservoirs at hydrostatic pressure. When considering the classical wedge-shaped structure of a foreland fold-thrust belt, one might expect deeply sourced fluids to be able to migrate long-distances along the decollement surface from hinterland areas of high stresses and crustal depths associated with metamorphic dehydration reactions towards the foreland. However, a growing body of evidence suggests that the vast quantities of fluids present in shallow sedimentary fold-thrust wedges are surface-derived (e.g. Burtner and Nigrini, 1994; Bebout et al., 2001; Wiltschko et al., 2009; Lynch and van der Pluijm, 2016), so perhaps fluids are instead driven by topographic gradients between mountain range interiors towards areas dominated by basins (e.g. Person et al. 2007).

Robust evidence exists for the widespread presence of surface-derived fluids in the brittle upper crust, and for the infiltration of fluids to depth through open fractures and pore space, mediated by brittle deformation (e.g., Muir-Wood and King, 1993; Sibson, 1994). In the case of fold-and-thrust belts, many studies focus on geochemical signatures of vein filling minerals near major deformation-related structures (e.g. Bebout et al., 2001; Kirschner and Kennedy, 2001; Rygel et al., 2006; Wiltschko et al., 2009). Calcite veins are often depleted in the heavy isotope of oxygen (or hydrogen) relative to their host rock, suggesting the infiltration of meteoric waters and their isotopic exchange with the host material (Nesbitt and Muehlenbachs, 1991; Kirschner and Kennedy, 2001; Clauer et al., 2013). Though these studies often suggest that external fluids are surface-derived, the original oxygen isotopic composition ($\delta^{18}O$) of those fluids is difficult to ascertain due to the fact that $\delta^{18}O$ values within the fluids are increasingly rock-buffered

with increasing fluid-rock interaction (Clauer et al., 2013). Because hydrogen is less abundant in crustal rocks, the hydrogen isotopic composition (δD) of the fluid does not undergo the same degree of rock buffering as $\delta^{18}O$. Secondly, the application of veins for fluid history implies synchronicity of fracture filling and main deformation pulses, which is uncertain until veins are dated. Instead, neoformed host rock grains constrain any temporal connections, which is a major motivation for targeting clays in this study.

Studies of the hydrogen isotopic composition of white micas in detachment faults have been successfully used to trace the infiltration of surface fluids down to the brittle-plastic transition (e.g. Mulch et al., 2004; Campani et al. 2012; Gebelin et al. 2013; Haines et al., 2016). Building on the use of phyllosilicates as fluid indicators, several recent studies have explored the utility of brittle fault and fold-hosted clay minerals to study upper crustal fluids (Hetzel et al. 2013: Fitz-Diaz et al., 2014; Boles et al. 2015; Mancktelow et al. 2016; Haines et al., 2016; Lynch and van der Pluijm, 2016). This study capitalizes on recently developed techniques and expands the use of clay mineral isotopic studies to include clay-rich cleavage seams, integrating the three settings (fault, fold, and cleavage-hosted clays) to study the syn-orogenic hydrologic regime in the Sevier fold- and thrust belt of Idaho and Wyoming.

Geologic Background

The Wyoming salient of the Sevier belt is characterized by thrust faults and folds that shortened and translated sedimentary cover rocks overall eastward during Early Cretaceous to Paleogene time (Figure III.1A; Wiltschko and Dorr, 1983; Royse, 1993; Yonkee and Weil, 2015). Major thrusts in the salient include a western system comprising the Willard, Paris, and Meade thrusts that carried thick Neoproterozoic to

Paleozoic passive margin strata, and an eastern system comprising the Crawford, Absaroka, and Hogsback-Darby-Prospect thrusts that carried thinner Paleozoic to Mesozoic platform strata. Cross sections of the salient show classic thin-skinned structures, constrained by seismic and drill-hole data (Figure III.1B; Royse, 1993).

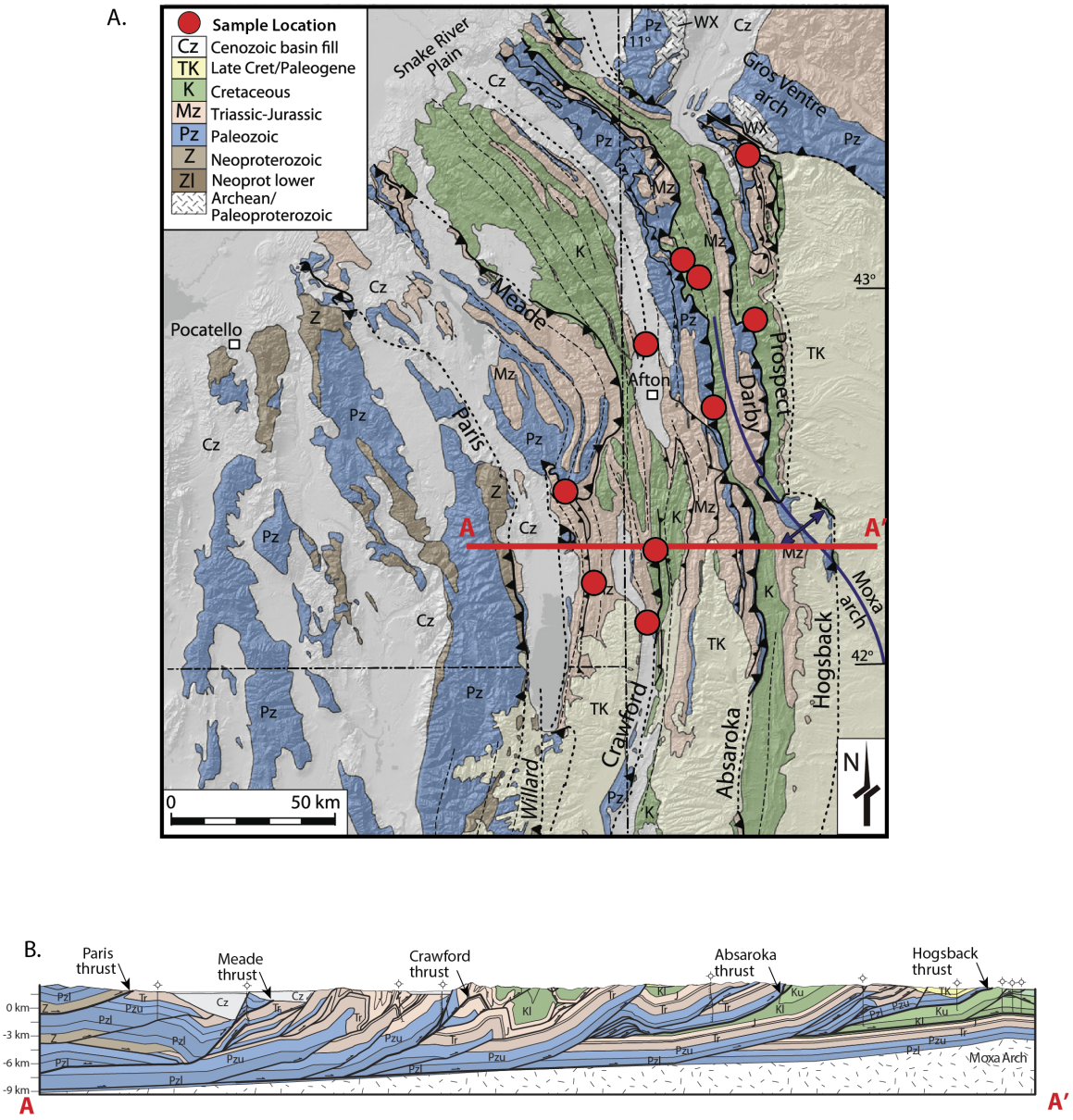

Figure III.1: a) Simplified geologic map of the Idaho-Wyoming salient of the Sevier fold-thrust belt (after Yonkee and Weil, 2015). Red circles show the locations of the collected clay samples. b) The E-W cross section from A to A' shows the generalized structure of the belt.

Thrusts have ramp-flat geometries, and are associated with large-scale fault-bend, fault-propagation, and detachment folds. The basal decollement lies in micaceous Neoproterozoic strata for the western thrust system, and in Cambrian shale for the eastern system.

Characteristics of syn-orogenic strata (e.g., Wiltschko and Dorr, 1983; DeCelles, 1994) and limited thermochronologic and geochronologic data (Burtner and Nigrini, 1994; Solum and van der Pluijm, 2007; Painter et al., 2014) constrain the long-term record of thrust timing. It has been proposed that the Willard-Paris-Meade thrusts were active from ca. 125 to 90 Ma, the Crawford thrust and associated fold train was active from ca. 90 to 80 Ma, motion on the Absaroka thrust occurred in two phases at ca. 80 Ma and ca. 70 to 60 Ma, and the frontal Darby-Prospect-Hogsback thrust was active from ca. 60 to 50 Ma (Figure III.2), recording multiple pulses and an overall forward propagation of the wedge front. Development of listric normal faults that locally reactivated thrust ramps and deposition of volcaniclastic strata in half grabens started by ca. 45 Ma, marking a switch to extensional collapse of the Sevier belt (Constenius, 1996).

Major fault zones typically include a damage zone near the base of the hanging wall comprised of variably deformed strata cut by multiple vein and minor fault sets, a rarely exposed fault core comprised of cataclasite and gouge with discrete slip surfaces, and sheared footwall rocks (Figure III.3). Cataclasite contains comminuted fragments that are locally re-cemented and re-brecciated, clay-rich seams, and multiple sets of microveins (Yonkee and Weil, 2015).

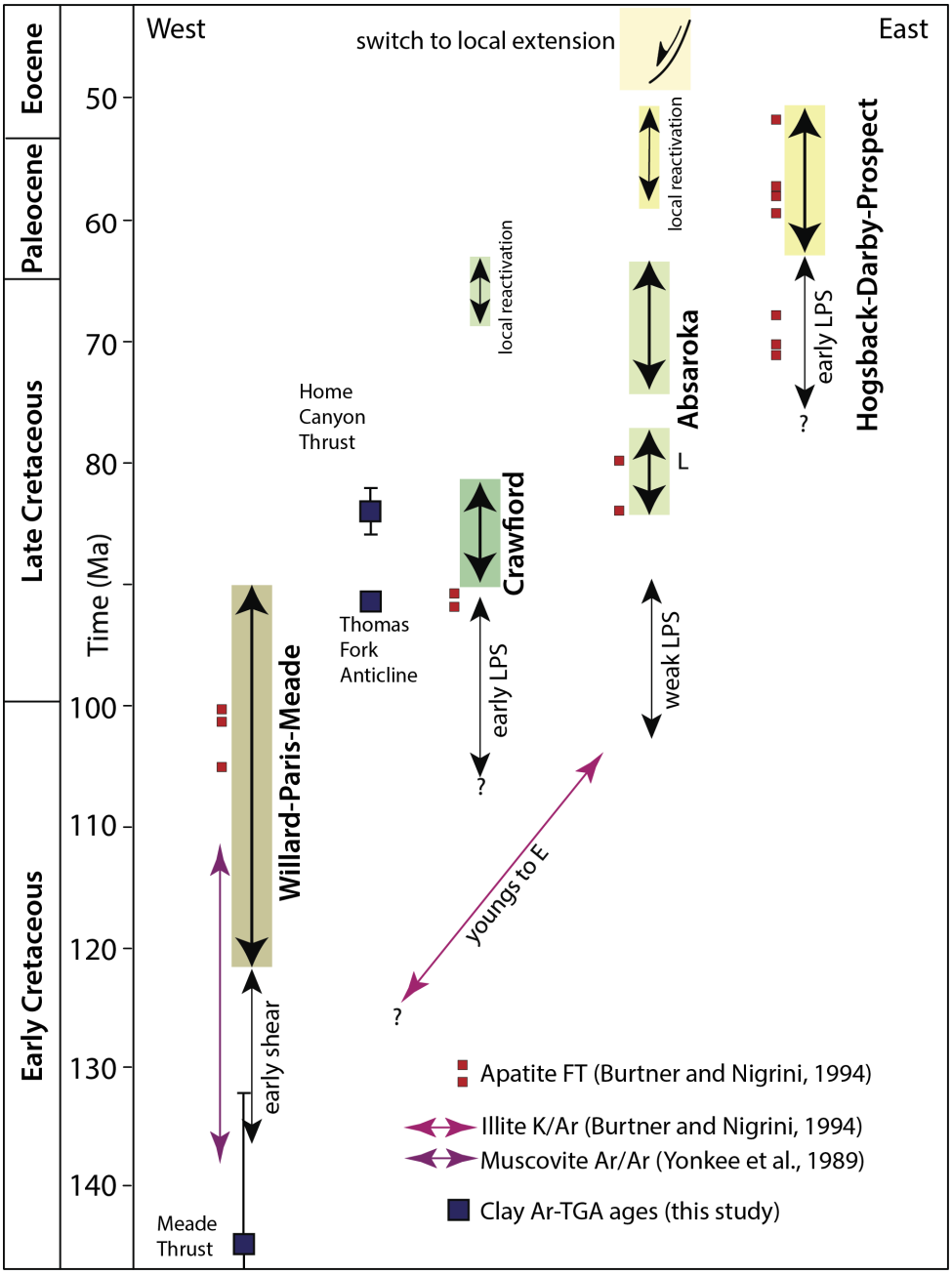

Figure III.2: Timing of major fault activity in the fold-thrust belt (after Yonkee and Weil, 2015). Ar-Ar-ages of fine-grained clay fractions from this study are shown as purple squares.

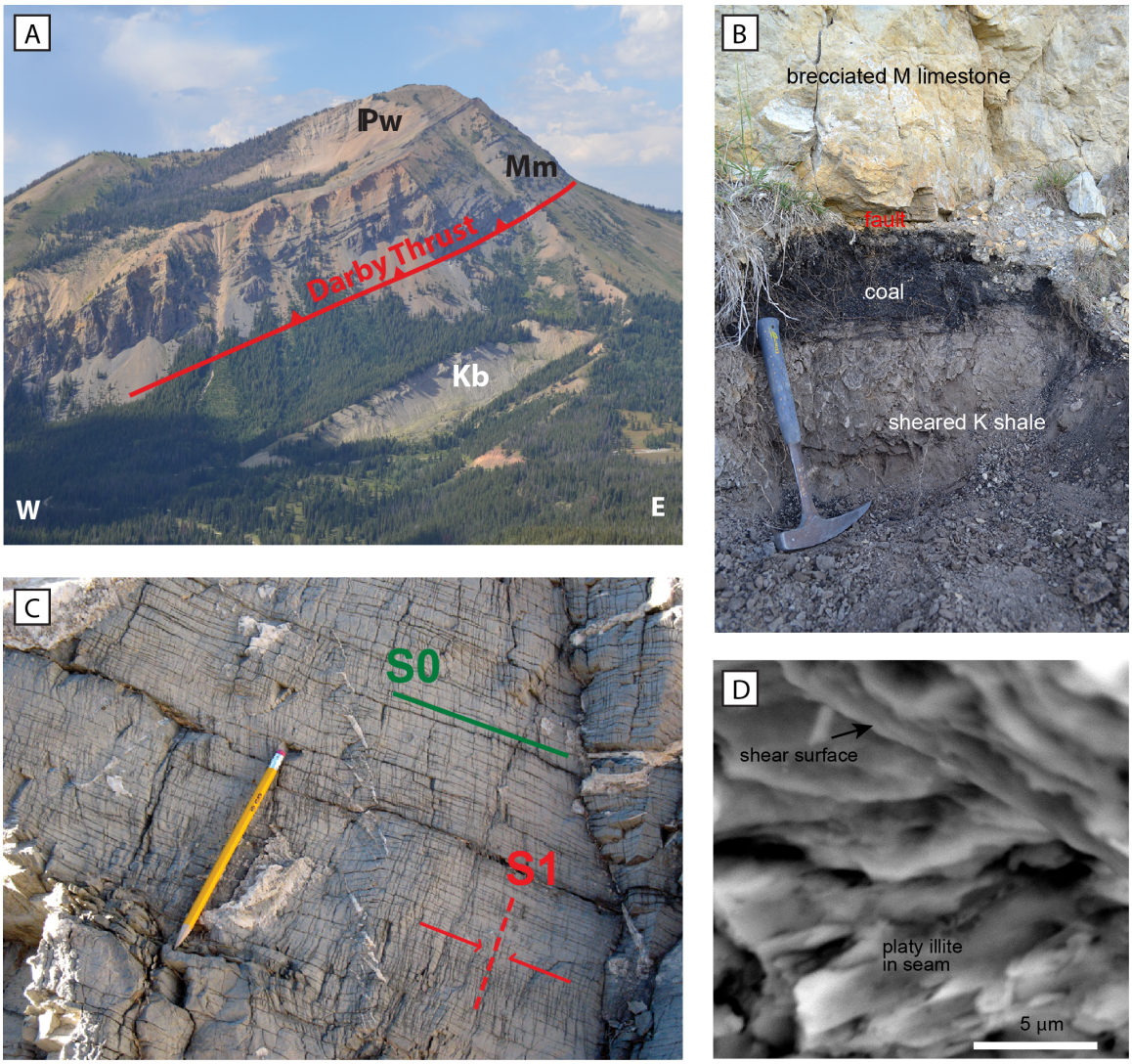

Figure III.3: a.) Overview photo of the Darby thrust. b.) Darby thrust fault outcrop. c.) Clay-rich cleavage seams in the Mississippian Madison formation in the Meade thrust hanging wall. d.) Scanning electron microscopic image of a sheared cleavage seam.

Mesoscopic structures in the eastern thrust system include spaced cleavage, vein sets, and minor faults (Mitra and Yonkee, 1985; Craddock, 1988; Yonkee and Weil, 2010). Cleavage, best developed in argillaceous limestone of the Jurassic Twin Creek Formation, is typically at high angles to bedding and perpendicular to the shortening direction defined by shapes of deformed fossils, recording early layer-parallel shortening (LPS) (Mitra and Yonkee, 1985). Microscopically, cleavage is represented by seams enriched in clay and quartz that formed mostly by dissolution of calcite (Figure III.3). Calcite was partly re-precipitated in veins, which include: a set parallel to bedding that accommodated minor vertical extension during early deformation, a dominant set of steep veins sub-perpendicular to structural trend (cross-strike set) that accommodated tangential extension during early to late stages of deformation, and a set parallel to cleavage seams that formed along steep fold limbs during late-stage deformation. Minor fault sets include conjugate wedge faults at acute angles to bedding that accommodated early LPS, conjugate tear faults at high angles to bedding that accommodated early to late wrench shear and tangential extension, and late bed-parallel and reverse faults that accommodated flexural slip and differential rotation of limbs during large-scale folding. Kinematic and cross cutting relations of mesoscopic structures and major fault zones record progressive concentration of deformation along larger, more throughgoing structures within individual thrust sheets (Yonkee and Weil, 2010).

Methods

Sampling Strategy

Samples of clay-rich materials were collected from a combination of major fault zones and spaced cleavage associated with internal deformation across the Wyoming salient (Figure III.1, Table III.1). Samples from major fault zones include (1) clay-rich seams from sheared Mississippian limestone in the damage zone of the Meade thrust (W15-87), (2) sheared Triassic red beds in the damage zone of the Home Canyon thrust—an imbricate of the Meade thrust (M-An-1), (3) poorly exposed, sheared Cretaceous shale from the damage zone of the Crawford thrust (W16-1G), (4) gouge from the fault core of the Absaroka thrust (W15-275), (5) sheared Cretaceous shale from the footwall exposed farther north (A-A-1), (6) sheared Cretaceous shale adjacent to the fault core of the Darby thrust (Dt-1b), and (7) sheared Triassic red beds near the Bear thrust—an imbricate of the Prospect thrust (A-2). Samples from cleavage in Jurassic limestone include clay-rich seams collected along the (8) Thomas Fork (W15-163A) and (9) Grover anticlines (W15-187A) in the Crawford sheet, and sheared seams collected along the (10) Grays River anticline (W13-35) in the Darby sheet.

Table III.1: Summary of δD data

Sample Name	Sample Description	δD of $1M_d$ Illite End-member	δD of coarse clay End-member
A-2	Bear thrust footwall, minor fault in Triassic red beds	-92.8 ± 1.6 ‰	-90.8 ± 5.8 ‰
A-A-1	Absaroka thrust footwall, sheared Cretaceous shale	-93.3 ± 1.6 ‰	-110.9 ± 5.4 ‰
M-An-1	Home Canyon thrust, minor fault in Triassic red beds	-91.6 ± 1.4 ‰	-86.3 ± 4.4 ‰
W13-35	Greys River anticline, sheared cleavage seam	-90.3 ± 1.8 ‰	-95.9 ± 8.7 ‰
W15-87	Meade thrust, sheared Mississippian limestone	-97.2 ± 3.2 ‰	-65.8 ± 9.3 ‰
W15-163A	Thomas Fork anticline, cleavage seam	-79.6 ± 1.6 ‰	-74.3 ± 5.2 ‰
W15-187A	Grover anticline, cleavage seam	-78.8 ± 1.7 ‰	-86.1 ± 5.0 ‰
W15-275	Absaroka thrust, fault core	-84.0 ±1.9 ‰	-62.6 ± 5.7 ‰

Clay Mineral Characterization

Samples were disaggregated by hand using an agate mortar and pestle, and four clay-size fractions, <0.05, 0.05-0.02, 0.2-1.0, and 1.0-2.0 μm, were separated by high-speed centrifugation. To characterize clay mineralogy with x-ray diffraction (XRD) analysis, both oriented slides and random powder mounts were prepared for each size fraction using the suspension and top-loading methods, respectively (see Lynch and van der Pluijm, 2016 for details). Clay slides and mounts were analyzed on a Rigaku Ultima X-Ray Diffractometer with a Cu source and a Ni foil k-beta filter, with a scanning speed of 1°/minute from 2 to 40° 2θ and step size of 0.05°2θ used for oriented slides. Oriented slides emphasize *(001)* peaks and are preferred for primary identification of clay mineral phases (illite, kaolinite, chlorite, smectite, interlayered phases). Relative proportions of clay mineral phases were quantified by comparing the relative intensities of *(00l)* peaks in accordance with the Mineral Reference Intensities method (see Lynch and van der Pluijm, 2016 for details). Random powder mounts were analyzed with a high-resolution step size of 0.02° 2θ and a scanning speed of 0.3°/minute, to evaluate proportions of high-temperature ($2M_1$) and low-temperature ($1M_d$) polytypes of illite. XRD patterns of two clay standards, the Owl Creek $2M_1$ muscovite and the Clay Minerals Society 1Mt-1 illite, were collected under identical conditions during the same analytical session. XRD patterns were input into a spreadsheet mixing routine and visually matched with sample patterns to determine the proportions of $2M_1$ and $1M_d$ polytypes in each size fraction. Error in this method is estimated to be approximately 2-3% (Haines et al., 2012).

Hydrogen Isotopic Analysis

Hydrogen isotope values were measured at the Joint Goethe University - Senckenberg BiK-F Stable Isotope Facility, Frankfurt, Germany. Results are reported in δD-notation relative to standard mean ocean water (SMOW). Approximately 1 mg of each size-fraction aliquot was encapsulated in Ag foil and dried overnight under vacuum at ~150°C. Prior to analysis, samples were rapidly transferred to a zero-blank auto sampler, which was purged with helium gas to prevent adsorption of atmospheric moisture to the sample material. δD values were measured on a ThermoFinnigan MAT 253 mass spectrometer in continuous flow mode coupled to a high temperature conversion elemental analyzer (TC-EA). In-house standards were run under same laboratory conditions, with an error less than ±2‰.

$^{40}Ar/^{39}Ar$ Analysis

Five samples were selected for $^{40}Ar/^{39}Ar$ illite geochronology. For each of these samples, fine (<0.05 μm) fractions were vacuum encapsulated into silica vials prior to irradiation at the McMaster Nuclear Reactor. During irradiation, recoil effects cause ^{39}Ar that is produced from ^{39}K in close proximity to grain boundaries to be lost from the crystal structure (Hall, 2014). This effect is insignificant for large-grains, since the fraction of recoiled argon is relatively small; for clay-sized grains, however, the amount of recoiled ^{39}Ar is significant and can commonly be up to 30%. Thus, encapsulation, which allows for the trapping and measurement of the recoiled gas fraction, is necessary for the accurate age determination of fine-grained samples (e.g. Hall, 2014). Irradiated samples were transferred to a vacuum line and measured on a VGS1200s mass spectrometer in the Noble Gas Laboratory at the University of Michigan. Under ultra-

high vacuum, silica vials were broken and the recoiled ^{39}Ar gas fraction was measured prior to the laser step-heating of the sample. We report total gas ages (TGAs), which represent the calculated age of the sample including both the recoiled and retained fraction or ^{39}Ar gas (Hall, 2014), based on crystallite sizes less than 12nm for $1M_d$ illitic clays in these rocks.

Results

Mineralogy

Eight of the ten samples contain clay fractions that are dominated by a single clay phase, namely illite, which makes them appropriate for hydrogen isotope analysis. Results of the polytype matching show that coarser fractions of these samples contain more of the $2M_1$ polytype (considered to be detrital illite), whereas the finer fractions contain abundant $1M_d$ polytype (low-temperature, authigenic illite that grew during deformation). Several of the samples contain minor chlorite in addition to illite. Coarser fractions of some samples also contain minor quartz and calcite, but presence of these non-hydrous minerals does not complicate H isotopic analysis. Samples from the poorly exposed damage zone of the Crawford thrust (W16-1G) and from the Darby thrust (DT-1B), however, contain significant amounts of smectite and kaolinite that negate meaningful H-isotopic analysis, and are thus not considered further. Typical XRD patterns for varying size fractions within a sample are shown in Figure III.4.

Hydrogen Isotope Data

Eight samples, seven of which have five size-fraction aliquots and one with four size-fraction aliquots, were analyzed. Coarser fractions generally have higher δD values, whereas fine fractions have lower δD-values, consistent with growth of fine-grained

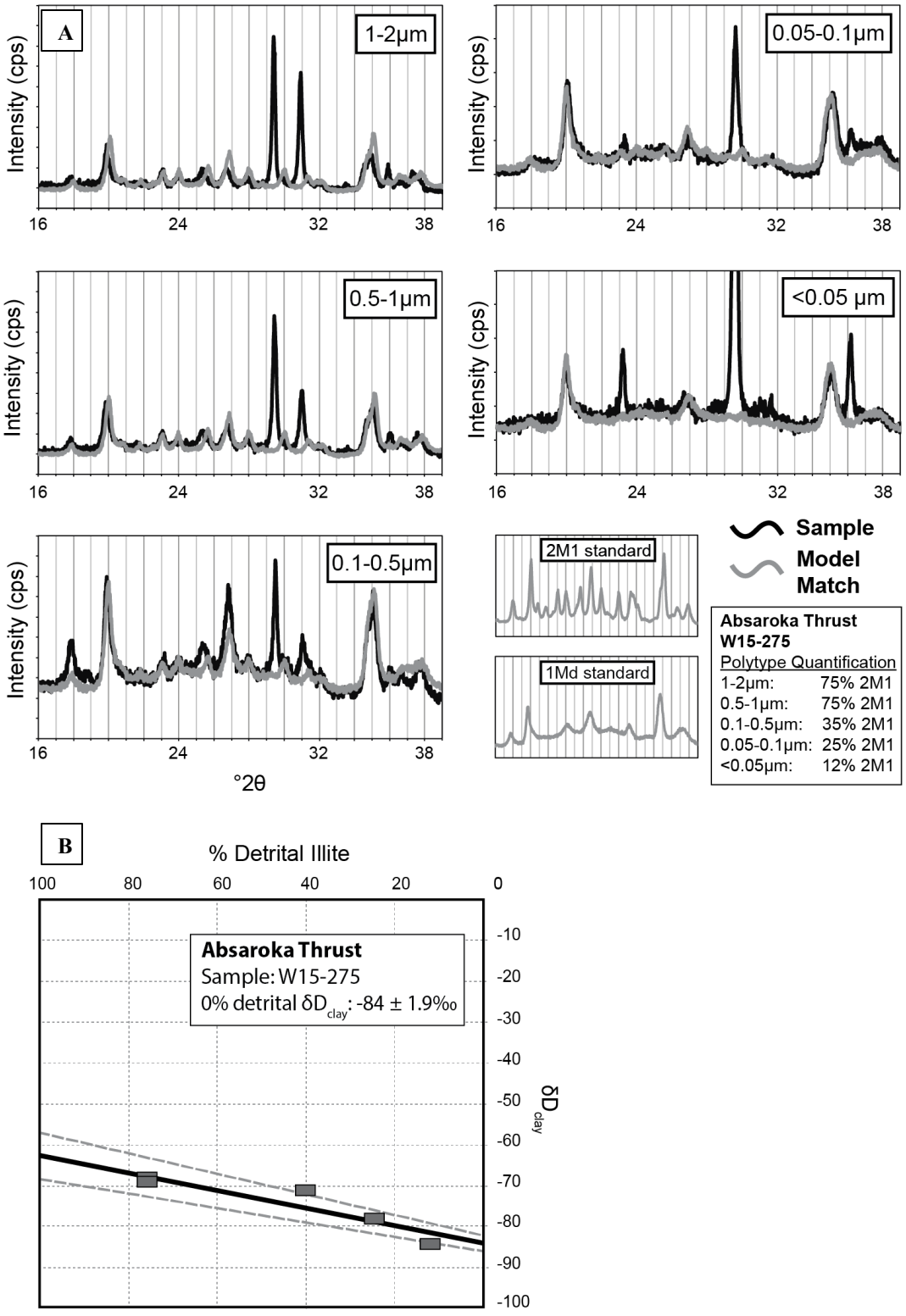

Figure III.4: Analyses from the Absaroka thrust sample, W15-275. A) XRD patterns and standards used for polytype characterization so an increasing proportion of low-temperature illite ($1M_d$) with decreasing grain size. B) Results of least-squares regression showing the hydrogen isotopic composition (δD value) of the end-member authigenic illite population and associated error envelope. Errors in the X and Y directions are contained within the boxes.

authigenic clays in the presence of low δD fluids (Figure III.5). Some samples have relatively constant δD values across all size fractions, consistent with growth of fine-grained clays and H isotopic exchange with locally buffered fluids. δD values for end-member $2M_1$ and $1M_d$ polytypes are estimated by linear least-squares regression, with weighting factors based on uncertainties in both the $1M_d$ proportions and measured δD values (Figure III.5B).

Calculated δD values for the authigenic $1M_d$ end member are highly negative for all samples from major fault zones, ranging from: -97.2±3.2‰ for the Meade thrust and -91.6±1.4‰ for the imbricate Home Canyon thrust; to -84.0±1.9‰ and -93.3±1.6‰ for samples from the Absaroka thrust fault core and sheared footwall shale, respectively; to -92.8±1.6‰ for the deformed footwall of the eastern, frontal Bear thrust. Two samples of cleavage seams that developed during early, internal deformation in the Crawford sheet have slightly less negative values of -78.8±1.7‰ and -79.6±1.6‰, whereas a sample of a sheared cleavage seam from a fold in the Darby sheet has a value of -90.3±1.8 ‰. End-member δD values for coarse clay fractions range from -110.9±5.4‰ to -62.6±5.7‰. The range of values reflect the mixing several populations of coarse clay grains and are difficult to interpret, in part because we are unable to determine the timing of detrital clay formation, which may be primary, diagenetic, or weathering-induced. For this reason, they are also not able to be used as provenance indicators. That the range of authigenic illite δD values is more restricted indicated that the record the conditions of their secondary formation from Sevier deformational fluids.

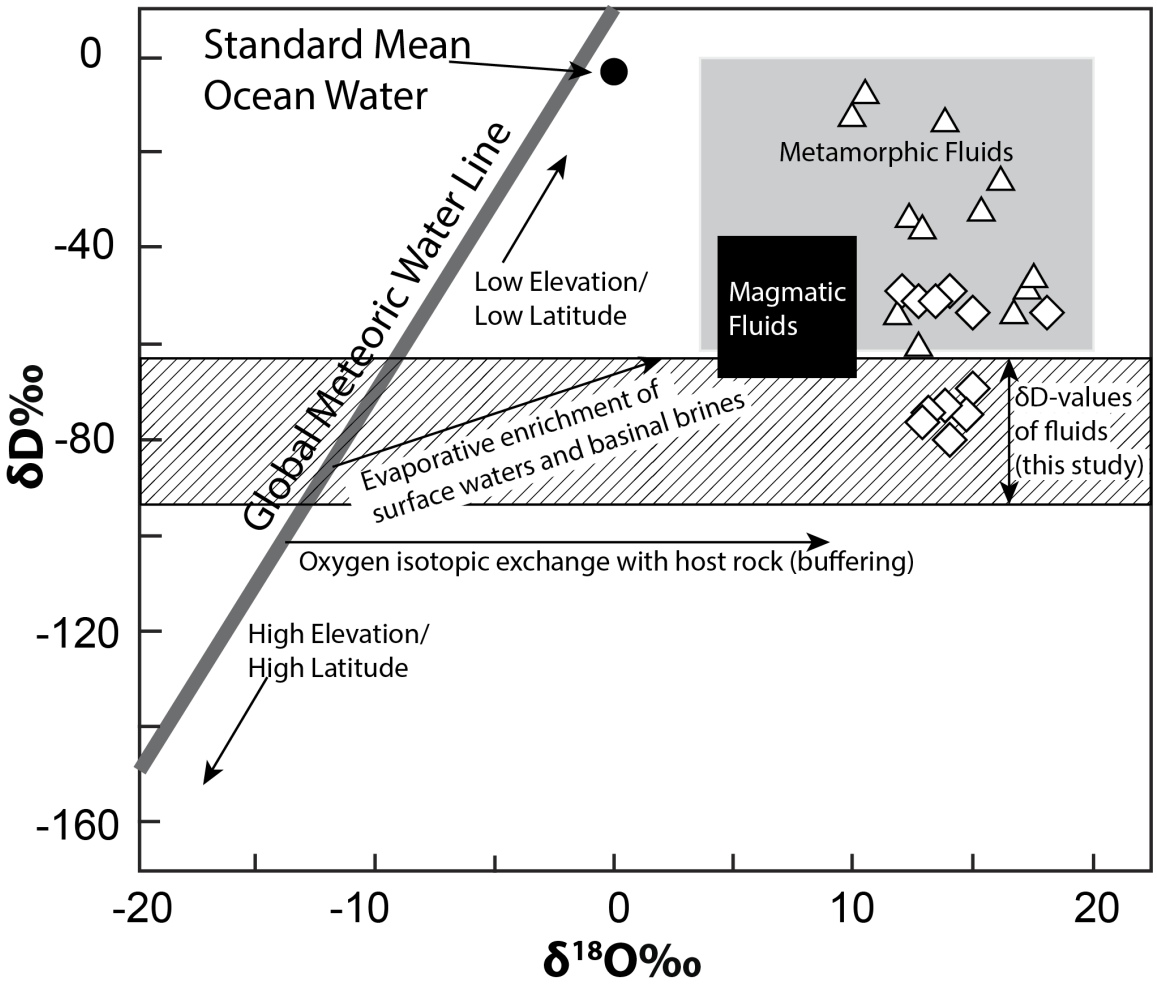

Figure III.5: Plot showing the composition of geologic fluids in oxygen and hydrogen stable isotope space (after Sheppard, 1986). Arrows indicate trends in the changing isotopic values of fluids with various physical processes. The range of δD_w values calculated in this study are shown in the textured box. White triangles and diamonds illustrate δD values of bulk illite in the Nugget Formation from the foreland basin and thrust belt, respectively, reported in Burtner and Nigrini (1994).

$^{40}Ar/^{39}Ar$ Ages

$^{40}Ar/^{39}Ar$ geochronology of four samples shows that neoformed clays are ancient and not reflecting growth from modern fluids or resetting from modern heating (Table III.2). Total-gas ages of fine fractions (<0.05 um) are composite ages that reflect mostly authigenic $1M_d$ illite, along with small portions of $2M_1$ illite. Two samples (M-An-1 and W15-163A) have Late Cretaceous ages for fine-grained illite interpreted to record late, thrust-related deformation, and two samples (W15-87 and W15-275) have Early

Cretaceous to Jurassic ages interpreted to represent populations of illite that grew during both early burial diagenesis and thrust-related deformation. End member ages of authigenic $1M_d$ illite in fine-grained fractions may be slightly younger than the reported total-gas ages due to the influence of small amounts (up to 12%) of older detrital $2M_1$ illite. In all cases, analyzed clays are ancient and did not form during interaction with modern fluids.

Table III.2: Illite proportions and ages of samples

Sample Name	Description	Detrital Illite	Total Gas Age
M-An-1	Home Canyon thrust, minor fault in Triassic red beds	0±3%	84.1 ± 1.7 Ma*
W15-163A	Thomas Fork anticline, cleavage seam	8±3%	91.3 ± 0.4 Ma
W15-87	Meade thrust, sheared Mississippian limestone	5±3%	145.7 ± 2.9 Ma*
W15-275	Absaroka thrust, fault core	12±3%	175.2 ± 1.3 Ma

*Corrected age (See Appendix B)

Discussion

Fluid δD Composition

δD values for the authigenic $1M_d$ end member illite are distinctly negative for all samples, ranging from -97 to -78‰ (VSMOW), and in most cases are lower than δD values for the detrital $2M_1$ illite component, indicating growth of authigenic illite in presence of low-δD waters. δD values for syn-deformational fluids are estimated using published illite-water fractionation factors (Capuano et al., 1992), and brackets on deformation temperatures (T) from available thermochronologic (Burtner and Nigrini, 1994), fluid inclusion (Wiltschko et al., 2009), and vitrinite reflectance data (Deming and Chapman, 1989). Paleo-depths of samples during thrust sheet burial and foredeep sedimentation, and paleo-thermal gradients both have large uncertainties, with gradients potentially ranging from ~20 to ~40 °C/km due to transient thermal effects associated with thrusting and advective heat transport by fluids. For cleavage samples from Jurassic

limestone, maximum T is ~150-180 °C at depths of ~5 to 6 km in the Crawford sheet, with slightly lower T and depths in the frontal Darby sheet. Fluid T along fault zones may have varied during transient upward and downward fluid flow, and a broad T range of 120-200 °C is considered for samples from fault cores and damage zones. Authigenic illite grains along fault zones may have grown during multiple episodes of fluid influx and alteration, and thus δD values of bulk samples represent an average of grains and fluids associated with clay growth. Cretaceous strata in the footwalls of major faults likely experienced T >100°C based on vitrinite reflectance data, but estimates have large uncertainties related to the rate of hanging wall erosion during thrust sheet emplacement. Brackets of estimated temperature and corresponding fluid δD_{fluid} values for each sample calculated using partition coefficients of Capuano et al. (1992) are given in Table III.3.

Table III.3: δD composition of illite and fluid

Sample Name	Sampled Material	δ D (‰) auth. illite	T (°C) bracket	δD (‰) fluid bracket
A-2	Triassic red bed, Bear thrust footwall	-92.8	140 to 170	-78 to -85
A-A-1	Sheared Cretaceous shale, Absaroka footwall	-93.3	120 to 150	-72 to -81
M-An-1	Triassic red bed, Home Canyon damage zone	-91.6	120 to 200	-71 to -90
W13-35	Jurassic limestone, sheared cleavage	-90.3	130 to 160	-73 to -80
W15-87	Mississippian carbonate, Meade damage zone	-97.2	120 to 200	-77 to -96
W15-163A	Jurassic limestone, cleavage seam	-79.6	150 to 180	-67 to -74
W15-187A	Jurassic limestone, cleavage seam	-78.8	150 to 180	-66 to -74
W15-275	Absaroka fault core	-84.0	120 to 200	-68 to -83

Fluids associated with formation of authigenic illite may have had deep (magmatic and metamorphic) or shallow sources (meteoric and formation waters). Deeply-sourced fluids typically have higher δD and/or $\delta^{18}O$ values whereas surface-derived fluids are typically characterized by lower δD and/or $\delta^{18}O$ values (Figure III.5;

Sheppard, 1986). Isotopic exchange with host rocks can quickly buffer oxygen isotopic composition, but because hydrogen content is low in rocks that are comprised mostly of anhydrous rock-forming minerals (quartz, calcite and feldspar), hydrogen isotopes do not undergo isotopic exchange as rapidly and are thus a more robust recorder of source fluid composition. Calculated δD_{fluid} values of fluids in equilibrium with authigenic illite range from ~ -66 to -96‰ (Table III.3). These values partly overlap with δD values of typical low-elevation meteoric waters, which range from ~-10 to -70‰ (Sheppard, 1986), yet contrast extremely negative δD values typical of high-elevation and/or high-latitude precipitation that has infiltrated fault zones in cores of orogenic belts (e.g. Poage and Chamberlain, 2001; Mulch et al., 2004; Mulch and Chamberlain 2007; Gébelin et al. 2012). As examined below, we interpret highly negative δD values of illite in our samples to record influx of surface-derived fluids, proposing that little-evolved basinal fluids were recharged by low-elevation, (near-shore) meteoric water, prior to and during deformation. Fluids are unlikely to include a magmatic component as igneous activity was absent in the study region, except for rare Eocene dikes that post-date thrusting. The nearest significant Cretaceous igneous activity was in the Idaho batholith, located ~300 km to the west, and even here incursion of meteoric waters was important during alteration and generation of ore deposits (e.g. Seal et al., 1993).

Evidence for Surface Fluid Involvement in Sevier Deformation

Surface-sourced fluids are ubiquitous in the shallow upper crust (<7km depth) as a result of evolving porosity and permeability that permit widespread fluid flow (e.g., Muir-Wood and King, 1993). Nevertheless, compressional environments, such as fold-

and-thrust belts, are commonly considered areas for significant expulsion of fluids from deeper crustal levels (Oliver, 1986; Koons and Craw, 1991).

Prior studies of veins and fluid inclusions indicated the presence of surface-sourced fluids in the shallow crust during Sevier orogenesis. In the Wyoming salient of the Sevier belt, Wiltschko et al. (2009) concluded that vein fill precipitated at near hydrostatic pressure, consistent with potential connection to near-surface meteoric-derived fluids along with interaction with locally-sourced formational fluids. Fluid pressures may have reached near lithostatic prior to and during vein propagation, with fluid pressure transients during episodes of sealing and compressive deformation followed by fracturing and opening of fluid pathways. Using stable isotopic studies of oxygen and carbon, Atnipp (1988) similarly identified surface-sourced meteoric fluid as a vein-forming fluid for a portion of Late Jurassic to Early Cretaceous veins in the Wyoming Overthrust Belt, though results from many vein populations were ambiguous regarding "tectonic" fluid origins. Within the Canadian Cordillera of Alberta, vein and fluid inclusion studies in the frontal fold-thrust belt also indicate infiltration of low-temperature, low $\delta D/\delta^{18}O$ fluids accompanying compressive deformation (Nesbitt and Muehlenbacks, 1991; Kirschner and Kennedy, 2001). Within the Idaho-Montana section of the Sevier belt, syn-tectonic veins and fluid inclusions likewise indicate the infiltration of surface-sourced waters to depths up to 10 km (Bebout et al., 2001; Rygel et al., 2006). Furthermore, Dworkin (1999) used isotopic composition of fault breccia to interpret deep infiltration of meteoric fluids into the rock units along and below thrust faults in Montana, subsequently ascending to the surface along these fault zones. The surface-derived fluids resided in fractures prior to their expulsion during thrusting, coming into

contact with and undergoing isotopic exchange with large volumes of rock (Nesbitt and Muehlenbachs, 1991; Kirschner and Kennedy, 2001; Clauer et al., 2013). Although low $\delta^{18}O$ values in veins indicate infiltration of a meteoric fluid source, the extent of isotopic exchange prior to vein precipitation and thus initial characteristics of source fluids, are difficult to estimate. In contrast, hydrogen is not a common rock-forming element and therefore, H-isotopes are better able to preserve the original characteristics of the primary surface fluids. In the following section, we explore surface stable isotopic records, in order to compare our hydrogen isotope data from deformed rocks to the compositions of Cretaceous-Paleogene meteoric and surface-derived fluids.

Surface Fluid Isotope Records

Currently available proxy records of the stable isotopic compositions of paleo-precipitation along the pre-Eocene North American Cordillera include secondary minerals (clays, carbonates) in paleosols, and fossils (freshwater bivalves, animal teeth). Deformation-related δD_{fluid} values estimated from authigenic illite in this study are compared with $\delta^{18}O_w$ values of meteoric waters estimated from pedogenic materials and fossils and equivalent δD_{equiv} values calculated using the global meteoric water line ($\delta D_{equiv} = 8*\delta^{18}O+10$) (Dansgaard, 1964). For the following discussion, we will include both the proxy $\delta^{18}O$ values reported in the literature and calculated δD_{equiv} values.

During the Late Cretaceous, the Western Interior Seaway abutted the foreland basin, and was a major source of precipitation on the eastern side of the Sevier belt (e.g. Fricke et al., 2010). Freshwater Unionid bivalves from the foreland basin preserve a bimodal distribution in $\delta^{18}O$ values, reflective of their depositional environments (Dettman and Lohmann, 2000; Fricke et al., 2008; Fricke et al., 2010; Foreman et al.,

2011; Tobin et al., 2014). Bivalves that grew in small ponds and streams record $\delta^{18}O_w$ of ~-7 to -11‰ (δD_{equiv} of -46 to -78‰) and are representative of low-elevation, near-shore watersheds, whereas bivalves that grew in larger rivers record negative $\delta^{18}O_w$ of <-15‰ (δD_{equiv} <-110‰) representative of high-elevation runoff including snowmelt (Figure III.6; Dettman and Lohman, 2000; Fricke et al., 2010). Bimodality may also partly reflect monsoonal climate patterns (Fricke et al., 2010, Foreman et al., 2011) as observed in soil carbonates (Foreman et al., 2011)

Proxies for Paleogene precipitation generally mimic those of the Cretaceous, though retreat of the Western Interior Seaway moisture source likely enhanced the 'distance effect' causing a negative shift in $\delta^{18}O_w$ and δD_{equiv} values (Dansgaard, 1964). Using three independent proxies—soil carbonate nodules, freshwater bivalves, and fossil teeth collected from the Bighorn Basin, Koch et al. (1995) estimated precipitation with $\delta^{18}O_w$ ~-8 to -12‰ (δD_{equiv} of -54 to -86‰) during the Paleocene and Eocene. Though there is a less pronounced bimodality in the distribution of $\delta^{18}O$ values of Unionid bivalves, studies show that the majority Paleocene-Eocene $\delta^{18}O_w$ estimates overlap with those of the low-elevation Cretaceous waters (Figure III.6; Dettman and Lohmann, 2000; Fan and Dettman, 2009). This also coincides with the calculated oxygen isotope composition of Cretaceous precipitation ($\delta^{18}O \cong$ -8‰ VSMOW) based on isotopic analysis of the lacustrian Petersen limestone unit (Atnipp, 1988).

Modern meteoric and surface fluids in the fold-and-thrust belt have lower δD and $\delta^{18}O$ values than those from Cretaceous or Paleogene times (Lawrence and Taylor, 1971; Bowen and Revenaugh, 2003), due to increased distance from the primary moisture source and cooler climate conditions and hence fractionation temperatures. Annual

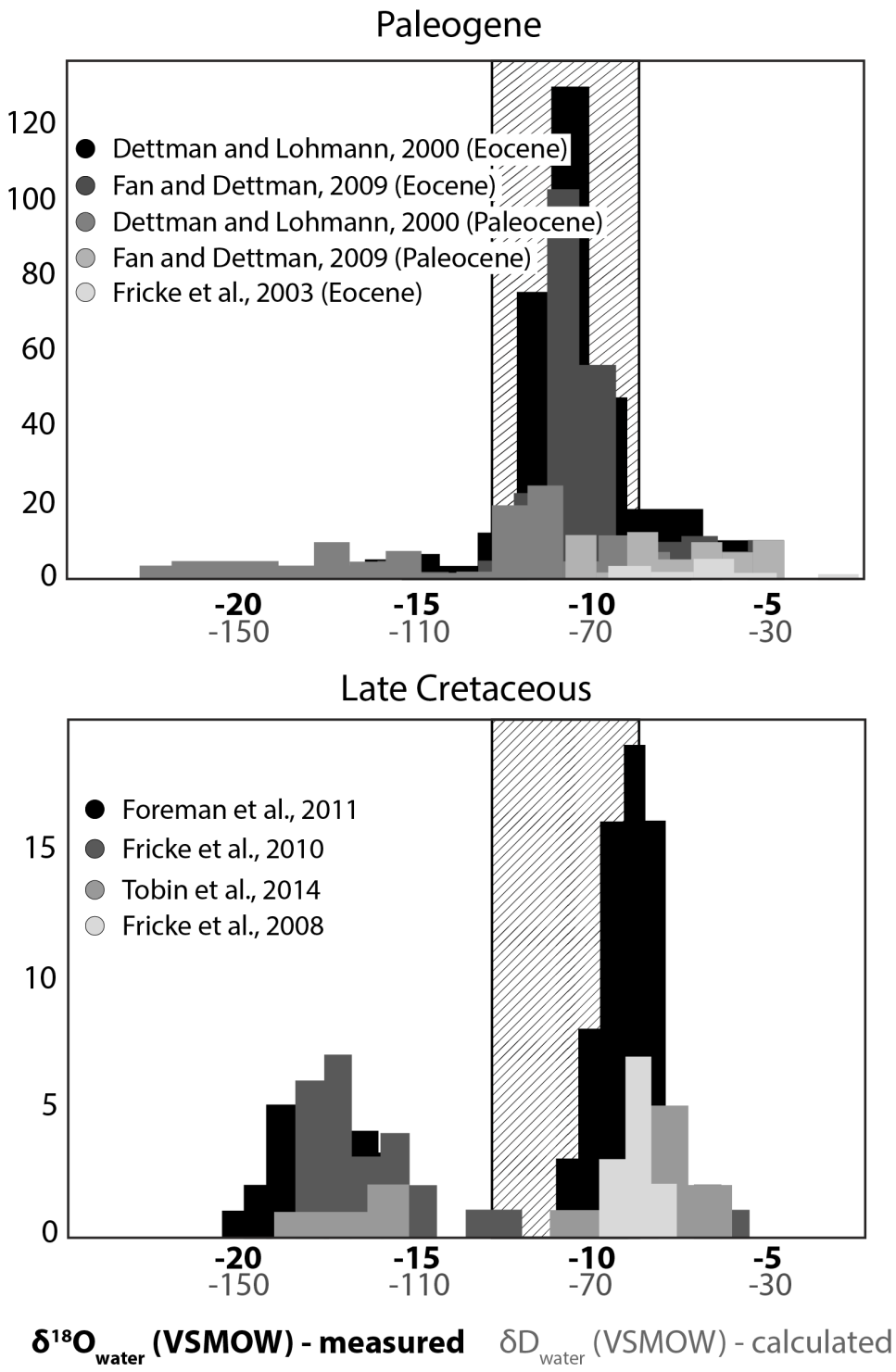

Figure III.6: Frequency distribution of Late Cretaceous and Paleocene surface water proxy isotopic composition from the Sevier foreland basin region. The bimodal pattern is prominent in the Late Cretaceous proxies, whereas, the Paleocene is dominated by a single large peak, shifted slightly toward more negatve δD values (lighter) relative to the larger of the two Late Cretaceous peak. As in figure III.5, the textured region in each diagram shows the range of δD_{fluid} range of calculated deformation fluids.

average $\delta^{18}O_{precipitation}$ in the study area ranges from ~-17‰ to -21‰, and $\delta D_{precipitation}$ ranges from ~-96‰ to -158‰ (Bowen and Ravenaugh, 2003). These ranges are incompatible with calculated δD_{fluid} values for authigenic illite, further supporting the conclusion that deformation-related clays record primary, deformation-related fluid conditions.

Ancient Surface Fluid in the Evolving Fold-Thrust Belt

To explain the presence of low-elevation, surface-sourced fluids in the Sevier fold-thrust belt, we test the following hypothesis: during the early stages of foreland basin uplift, sedimentary units experienced permeability increases associated with deformation, resulting in the incursion of local meteoric fluids into the basin sediments (Figure III.7). This phenomenon has been observed in several cases, and is especially pronounced along basin margins and in association with faults (Glasmann et al., 1989; Hayes and Boles, 1993). This scenario is supported by thermochronometry results from the Idaho-Wyoming Sevier belt, which indicate a contemporaneous zone of rock cooling, interpreted as the result of meteoric fluid recharge into the active thrust units and the proximal foreland basin sediments (Burtner and Nigrini, 1994). Connolly and Podladchikov (2004) presented a mechanism by which buoyancy forces in compressional regimes can cause surface-sourced fluids to migrate downward to a zone of neutral buoyancy at ~2-4 km depth, roughly similar to the estimated depths of illite formation. Wiltschko et al. (2009) also pointed to possible wholesale resetting of $\delta^{18}O$ values in carbonates of the Twin Creek Formation by infiltration of low $\delta^{18}O$ fluids sometime prior to deformation.

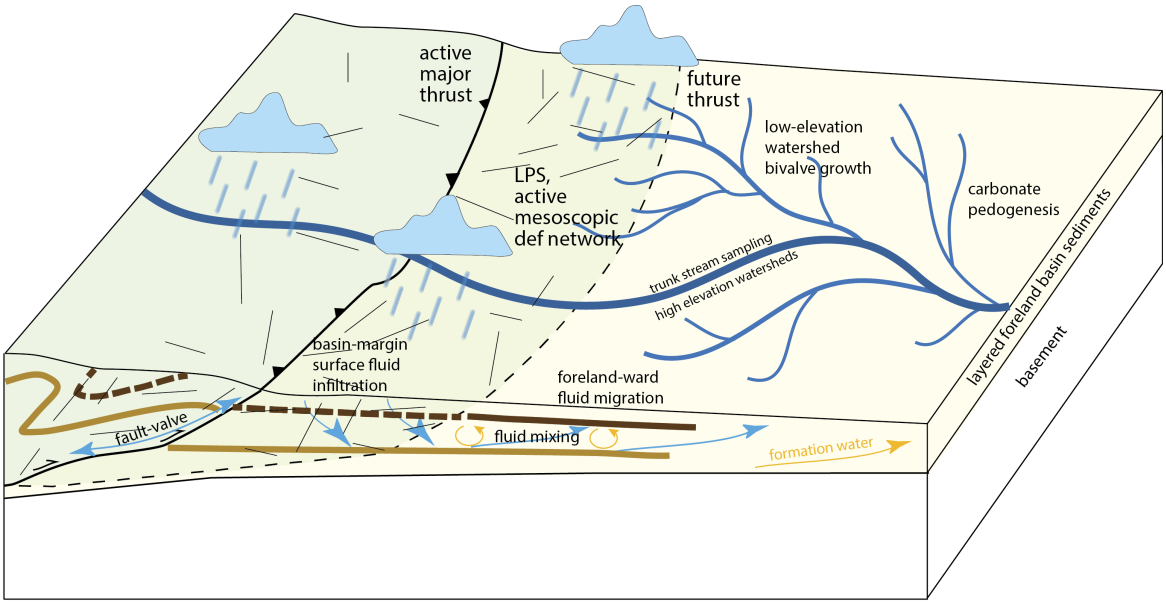

Figure III.7: Conceptual diagram of fluid flow in the Sevier thrust belt. Low elevation meteoric water recharges at the actively deforming basin margins and flows with formation water toward the foreland. The dark blue trunk stream samples higher elevation precipitation, whereas the light blue streams sample low-elevation meteoric waters. The active major thrust acts as a barrier to cross-fault flow.

During the onset of compressional deformation, fluids were expelled during faulting, migrating both along and away from the fault zone (toward the foreland), promoting the mineralization of low-temperature illite (e.g., Oliver, 1986; Dworkin, 1999). Fluid flow accompanying faulting has been described in terms of a fault-valve mechanism (Sibson, 1994), which is characterized by transient permeability changes in the fault zone throughout the rupture cycle. In the case of compressional faulting, fluids in the fault zone are slowly expelled as pore space and permeability are reduced along the fault plane when local stresses build (Sibson, 1994; Evans et al., 1997). Following a rupture event, which relieves the local stresses, fracture density is increased and pore spaces are able to open again, increasing permeability and allowing the return of mineralizing fluids to the fault zone (Sibson, 1994; Evans et al., 1997). Over time, mineral growth in the fault zone reduces the permeability and creates an impermeable

barrier to cross-fault flow, which would inhibit the wholesale migration of the highest-elevation meteoric fluids to migrate to the frontal thrusts (Evans et al., 1997). Hence, low-elevation, and, in the case of the Sevier belt in the Idaho-Wyoming salient, nearshore surface fluids dominate the brittle fault fluid signatures recorded in neomineralized illite.

Conclusions/Summary

Our study of fluid signatures from ancient clays associated with thrusting and folding in the Sevier belt of the northwestern US shows that surface-sourced fluids were present in the upper crust during orogenesis. δD_{fluid} values calculated from both pre- and syn-deformational clay mineral δD_{clay} values show the presence of low-elevation meteoric fluids in sediments at crustal depths of approximately 3-4 km, just prior to and during regional contraction.

The preservation of ancient fluid compositions also provides evidence that hydrogen isotope compositions in deformation-related illite are a valuable tracer for determining the characteristics of mineralizing fluids. With surface-sourced fluids being the dominant fluid in these upper-crustal fault zones, δD provides a complementary method to study the isotopic composition of regional precipitation during the time of deformation, which has previously relied mostly on $\delta^{18}O$ characteristics of fossils and paleosols. Thus, authigenic illite characterization offers an additional alternative to carbonate surface water records, which have limitations due to e.g. isotope fractionation during evaporation of soil and lake water at the Earth's surface or diagenetic alteration within orogen interiors.

Acknowledgements

This chapter was submitted to *Earth and Planetary Science Letters* with the coauthorship of Andreas Mulch, Ben van der Pluijm, and Adolph Yonkee, The authors wish to thank John Craddock, John Geissman and Nathan Niemi for suggestions of field sampling, and Zhongrui Li and Chris Hall for assistance with laboratory analyses. Thanks also to Kyger Lohmann for discussions regarding K-T surface fluid proxies. This project was supported by the Society of Economic Geologists and by the Clay Minerals Society through Student Research Grants to Lynch and a National Science Foundation Grant (EAR-1450840) to Yonkee. Clay research at the University of Michigan is supported by the NSF, most recently under EAR-1629805. Additional support was provided by the University of Michigan's Turner Student Research Fund.